# ORIGINAL RESEARCH

Macrophage Raptor Deficiency-Induced Lysosome Dysfunction Exacerbates Nonalcoholic Steatohepatitis

Wenli Liu,[1],* Chenji Ye,[1],* Qian Cheng,[1] Xuejiao Zhang,[1] Liu Yao,[1] Qi Li,[1] Jing Huang,[1] Yajin Liu,[1] Zhengsheng Zou,[2] Hua Wang,[3] Jun Yan,[4] Yi Zhu,[1] Chunjiong Wang,[1] and Ding Ai[1]

[1]Tianjin Key Laboratory of Metabolic Diseases, Department of Physiology and Pathophysiology, Tianjin Medical University, Tianjin, China; [2]The Center for Non-infectious Liver Diseases, Beijing 302 Military Hospital, Beijing, China; [3]Department of Oncology, the First Affiliated Hospital, Institute for Liver Diseases of Anhui Medical University, Hefei, China; [4]Department of Pathology, Tianjin First Center Hospital, Tianjin, China
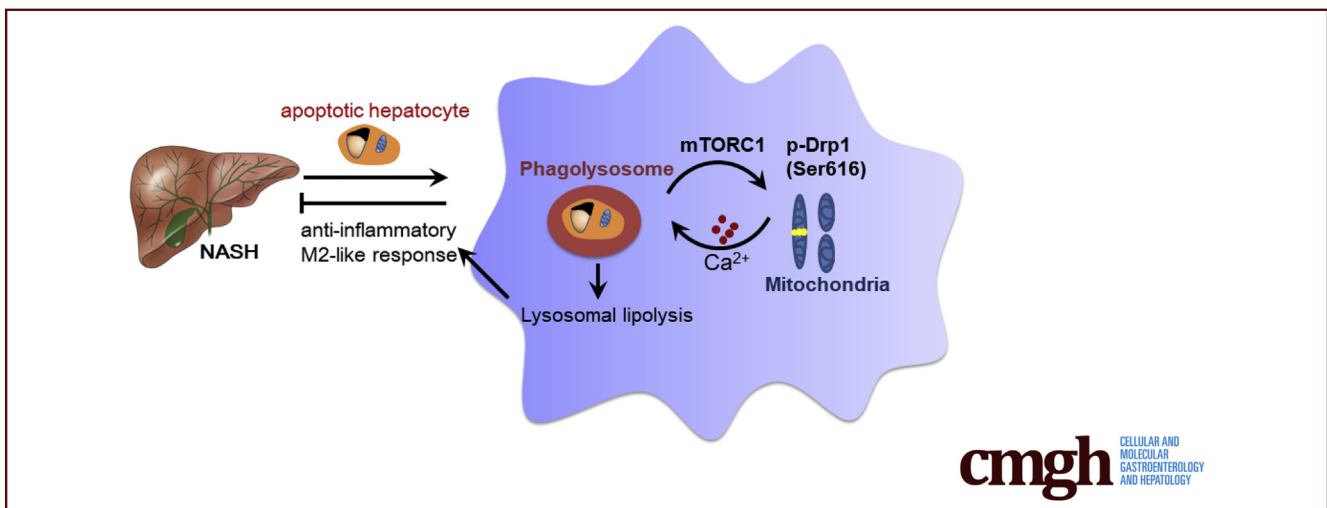
SUMMARY

Loss of mammalian target of rapamycin complex 1 activity in macrophages contributes to the progression of nonalcoholic steatohepatitis by attenuating M2-like response during clearance of apoptotic hepatocytes. In macrophages, the activation of mammalian target of rapamycin complex 1 during phagocytosis is responsible for dynamin-related protein –-mediated lysosomal lipolysis, which promotes the M2-like response.

BACKGROUND & AIMS: Nonalcoholic steatohepatitis (NASH) is an increasingly prevalent nonalcoholic fatty liver disease, characterized by inflammatory cell infiltration and hepatocellular damage. Mammalian target of rapamycin complex 1 (mTORC1) has been investigated extensively in the context of cancer, including hepatocellular carcinoma. However, the role of mTORC1 in NASH remains largely unknown.

METHODS: mTORC1 activity in macrophages in human mild and severe NASH liver was compared. Mice with macrophage-specific deletion of the regulatory-associated protein of mTOR (Raptor) subunit and littermate controls were fed a high-fructose, palmitate, and cholesterol diet for 24 weeks or a methionine- and choline-deficient diet for 4 weeks to develop NASH.

RESULTS: We report that in human beings bearing NASH, macrophage mTORC1 activity was lower in livers experiencing severe vs mild NASH liver. Moreover, macrophage mTORC1 disruption exacerbated the inflammatory response in 2 diet-induced NASH mouse models. Mechanistically, in response to apoptotic hepatocytes (AHs), macrophage polarization toward a M2 anti-inflammatory phenotype was inhibited in Raptor-deficient macrophages. During the digestion of AHs, macrophage mTORC1 was activated and coupled with dynamin-related protein 1 to facilitate the latter's phosphorylation, leading to mitochondrial fission-mediated calcium release. Ionomycin or A23187, calcium ionophores, prevented Raptor deficiency–mediated failure of lysosome acidification and subsequent lipolysis. Blocking dynamin-related protein 1–dependent mitochondria fission impaired lysosome function, resulting in reduced production of anti-inflammatory factors such as interleukins 10 and 13.

CONCLUSIONS: Persistent mTORC1 deficiency in macrophages contributes to the progression of NASH by causing lysosome dysfunction and subsequently attenuating anti-inflammatory M2-like response in macrophages during clearance of AHs. *(Cell Mol Gastroenterol Hepatol 2019;7:211–231; https://doi.org/10.1016/j.jcmgh.2018.09.011)*

Keywords: mTORC1; NASH; Lysosome; Drp1.

Nonalcoholic fatty liver disease (NAFLD) comprises a wide spectrum of diseases, including hepatic steatosis, nonalcoholic steatohepatitis (NASH), liver fibrosis, cirrhosis, and hepatocellular carcinoma (HCC).[1] Although only a minority of NAFLD patients (approximately 20%) are diagnosed with NASH, NASH subtypes can progress to advanced liver diseases, including cirrhosis and HCC.[2] From 2002 to 2012, the number of patients undergoing liver transplantation for HCC secondary to NASH increased by nearly 4-fold, as compared with the 2-fold increase caused by HCC; hence, NASH is predicted to become the leading indication for liver transplantation over the next decade.[3,4] Despite efforts to control NASH by pharmacologic or lifestyle interventions targeting insulin resistance, oxidative stress, and obesity,[5] the therapeutic efficiency still is limited. Therefore, identifying the molecular pathways that direct NASH progression are required to show new therapeutic approaches.

Mammalian target of rapamycin (mTOR) functions as a catalytic subunit of 2 functionally distinct complexes (mTORC1 and mTORC2). mTORC1 acts as a hub to integrate the upstream signals from nutrients, growth factors, and other stimuli. mTORC2 is involved in cellular metabolism as well as the cytoskeleton.[6] mTORC1 is a serine/threonine kinase that regulates various biological processes such as lipogenesis, protein synthesis, and autophagy, which phosphorylates the downstream effectors including translation initiation factor 4E-binding proteins, ribosomal protein S6 kinases, and UNC-51–like kinase 1.[6]

Our previous studies focused on the immune response in cardiovascular diseases,[7,8] and identified a pro-atherogenic role for macrophage mTORC1 in the development of atherosclerosis by increasing the production of chemokines. In addition to cardiovascular diseases, immune cells also play an essential role in the development of NAFLD from simple hepatic steatosis to NASH.[4] As dictated by a newly proposed multiple parallel hits hypothesis, once insulin signaling is impaired in the liver, extrahepatic inflammation might develop, owing to recruitment of innate immune cells such as macrophages and natural killer T cells in parallel to the hepatic steatosis.[9–11] Given the causal link between mTORC1 and inflammation, we hypothesized that macrophage mTORC1 plays an important role in NASH pathogenesis as well.

Tissue-resident Kupffer cells and recruited macrophages are essential components of innate immunity in the liver. They play a central role in local inflammation, orchestrate tissue remodeling, participate in various metabolic processes, and fulfill hepatic homeostatic functions.[10,11] In response to diverse environmental signals, macrophages express different functional programs, termed *macrophage polarization*. In general, 2 distinct macrophage subsets have been recognized, namely, the classic M1 macrophages and the alternative M2 macrophages. On exposure to lipopolysaccharide (LPS) or Th1 cytokines (interferon γ), macrophages are polarized to the M1 phenotype with high production of proinflammatory factors such as tumor necrosis factor α (TNFα), interleukin 6 (IL6), and inducible nitric oxide synthase (iNOS), whereas the alternative M2 macrophages are polarized by Th2 cytokines (such as IL4 and IL13), which participate in the resolution of inflammation.[12] Recent studies have found that polarized macrophages show distinct metabolic phenotypes, which contribute to their activation state. Increased aerobic glycolysis was observed in M1 macrophages, whereas fatty acid oxidation was observed in M2 macrophages.[12,13] Inhibition of fatty acid oxidation blocked M2 activation, but overexpression of peroxisome proliferator–activated receptor γ coactivator 1β significantly increased mitochondrial oxidative phosphorylation, which promoted the IL4-induced macrophage alternative activation and attenuated the proinflammatory cytokine production.[14] In addition, a recent study identified cell-intrinsic lysosome lipolysis as a critical source of fatty acids that fuel the M2-like response process.[12] However, little is known about the effect of metabolism-directed macrophage polarization on NASH.

While exploring these unknown questions, we observed lower macrophage mTORC1 activity in livers of patients with severe NASH vs mild NASH. Genetic suppression of mTORC1 activity exacerbated inflammation in mice with NASH without altering steatosis. Regulatory-associated protein of mTOR (Raptor) deletion in macrophages inhibited phagocytosis-induced macrophage polarization toward the M2 anti-inflammatory phenotype by impairing lysosome acidification and lipolysis. Disruption of mTORC1 suppressed dynamin-related protein 1 (Drp1) phosphorylation-induced mitochondria fission and subsequent calcium release to cytoplasm. Administration of calcium ionophores reversed the defective calcium-dependent vacuolar (H^+)-adenosine triphosphatase (V-ATPase) activity and increased lysosomal lipolysis. Mitochondrial division inhibitor 1 (Mdivi-1), a Drp1 inhibitor, mimicked the suppression of lysosomal lipolysis and the production of IL10 and IL13 of the Raptor deficiency in macrophages. Our findings show that the activation of macrophage mTORC1 during the digestion of apoptotic hepatocytes (AHs) might be a protective response to prevent the progression of NASH, which resolves hepatic inflammation during NASH.

Most current article

Results

mTORC1 Activity in Macrophages Is Lower in Severe Vs Mild NASH Human Liver Samples

To address the association of macrophage mTORC1 activity and the development of NASH in human beings, we tested the cell specificity of mTORC1 activity by the intensity of phospho-S6 staining in liver sections positive for the pan-macrophage marker CD68 obtained from patients with mild and severe NASH (Figure 1A and B). The phospho-S6 level in macrophages was lower in severe than in mild NASH livers (Figure 1C and D), but the total S6 level was comparable (Figure 1E and F), which reflects the reduced mTORC1 activity in severe NASH livers. However, in simple steatosis human liver, the macrophage p-S6 level is similar to that in mild NASH liver (Figure 1G and H). Although the change of the macrophage p-S6 level during the development of simple steatosis was unknown, these observations in human beings suggest that mTORC1 activity might be involved in the progression of NASH.

Persistent Disruption of mTORC1 in Macrophages Exacerbates a High-Fructose, Palmitate, and Cholesterol Diet– or Methionine- and Choline-Deficient Diet–Induced Steatohepatitis

To investigate the effect of macrophage mTORC1 on NASH, we crossed Raptor[flox] with LysMcre mice (Jackson Laboratory, Bar Harbor, ME) to generate myeloid cell lineage–specific Raptor-deficient (macrophage-specific Raptor-knockout mice [Raptor[MacKO]]) mice (Figure 2), and used the mice in various experimental models of NASH. First, Raptor[MacKO] and Raptor[flox] mice were fed a normal chow diet (NCD) or high-fructose, palmitate, and cholesterol (FPC) diet for 24 weeks. In both genotypes, body and adipose tissue weights were higher with the FPC diet than the NCD and did not differ between the 2 strains (Figure 3A). Insulin sensitivity, as reflected by intraperitoneal glucose tolerance testing, was impaired in Raptor[flox] mice fed the FPC diet vs the NCD but was not affected further by Raptor deficiency (Figure 3B). However, Raptor[MacKO] mice showed increased accumulation of multiple immune subsets in livers from mice fed the FPC diet (Figure 3C). With the FPC diet, the hepatic accumulation of macrophages (CD68- and Mac-3–positive cells) and plasma alanine aminotransferase (ALT) and aspartate aminotransferase (AST) levels were significantly induced in Raptor[MacKO] mice (Figure 3C–E).

In rodent models of NASH and in patients, the levels of inflammatory factors including cytokines and chemokines have been implicated in the pathogenesis of NASH.[15] Indeed, with the FPC diet, the hepatic messenger RNA (mRNA) levels of TNFα, monocyte chemoattractant protein 1 (MCP-1), and iNOS were higher in Raptor[MacKO] than Raptor[flox] mice (Figure 3F). However, lipid deposition in hepatocytes and hepatic triglycerides and cholesterol levels were similar between the 2 genotypes fed the FPC diet (Figure 3G and H).

We next explored the relevance of these findings in a second model of steatohepatitis. Raptor[MacKO] and Raptor[flox] mice at 8 weeks old were fed the NCD or the methionine- and choline-deficient (MCD) diet for 4 weeks. As previously reported,[16] in both groups, liver and body weights were lower with the MCD diet than the NCD (Figure 4A). Consistent with the FPC diet, after 4 weeks of the MCD, inflammatory cell infiltration, especially macrophages, was greater in Raptor[MacKO] than Raptor[flox] livers (H&E, CD68, and Mac-3 staining) (Figure 4B and C). As further evidence of inflammation, with the MCD diet, plasma ALT and AST levels and hepatic mRNA levels of TNFα, MCP-1, and iNOS were higher in Raptor[MacKO] than in Raptor[flox] mice (Figure 4D and E). However, hepatic lipid deposition was similar between Raptor[MacKO] and Raptor[flox] mice with the MCD diet (Figure 4F and G).

Raptor Deficiency in Macrophages Attenuated AH-Induced Macrophage M2-Like Response

We next sought to explore the reasons for advanced NASH in Raptor[MacKO] mice. Recruited macrophages and Kupffer cells play a critical role in hepatic inflammation in response to many mediators in plasma such as lipotoxic lipids and pathogen-associated molecular patterns[17] promoting the development of NASH.[10] We treated macrophages from Raptor[flox] or Raptor[MacKO] mice with serum (10%) from wild-type mice fed the NCD or MCD diet, as described previously. Serum from MCD-fed mice significantly induced the mRNA levels of TNFα and MCP-1 in both control and Raptor-deficient macrophages (Figure 5), which suggests the existence of inflammatory mediators in serum with the MCD diet. However, macrophages from the 2 genotypes showed a similar inflammatory response to the MCD serum (Figure 5), which implies a mechanism other than a direct immune response.

Hepatocellular apoptosis is an important histologic feature associated with NASH.[18,19] As a type of phagocyte, macrophages clear apoptotic cells to maintain liver homeostasis (Figure 6A).[20] Macrophages show an M2-like response to apoptotic cells. This response is fueled by fatty acids from cell-intrinsic lysosomal lipolysis.[12,13] Consistently, mRNA levels of IL10, IL13, and arginase-1, as well as glycerol levels in the medium, were increased in control macrophages after AH treatment, which was abolished by Raptor deficiency (Figure 6B and C). In line with in vitro data, with the FPC diet, the number of anti-inflammatory M2-like macrophages in the liver was lower in Raptor[MacKO] than in Raptor[flox] mice, as evidenced by a reduced CD68^{+}/CD206^{+} cell count (Figure 6D and E). In addition, hepatic mRNA levels of IL10 and IL13 also were lower in Raptor[MacKO] than in Raptor[flox] mice (Figure 6F). However, the IL4-induced expression of M2 macrophage genes was comparable between the 2 genotypes (Figure 6G). Therefore, Raptor deficiency attenuated AH-dependent polarization of macrophages toward an anti-inflammatory M2 phenotype.

Raptor-Deficient Macrophages Had Defects in Digestion of AHs

To ascertain the function of macrophage mTORC1 in clearing AHs, we investigated the process of phagocytosis in macrophages from Raptor[MacKO] and Raptor[flox] mice. We labeled the AHs with succinimidyl ester and incubated them

A

Mild NASH   Severe NASH

B
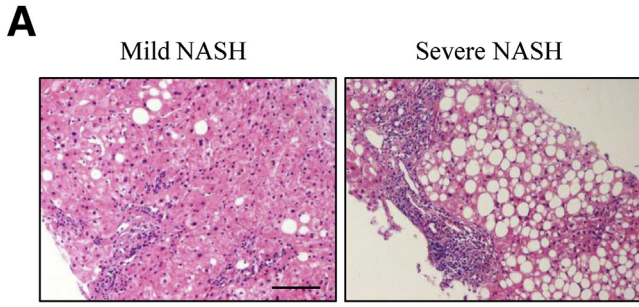
NAFLD Activity Score （mean+SEM）		
	mild	severe
Steatosis (0-3)	1.4 ± 0.25	2.6 ± 0.25
Lobular inflammation (0-3)	1 ± 0	1.8 ± 0.2
Ballooning (0-2)	1.8 ± 0.2	1.8 ± 0.2
Total (0-8)	4.2 ± 0.2	6.2 ± 0.37

C

p-S6   CD68   DAPI   Merge

Mild NASH

Severe NASH

D

E

S6   CD68   DAPI   Merge

Mild NASH

Severe NASH

F

G

p-S6   CD68   DAPI   Merge

Simple Steatosis

Mild NASH

H
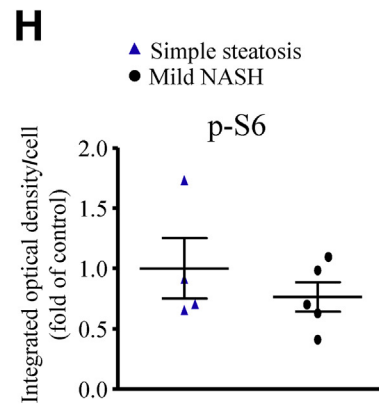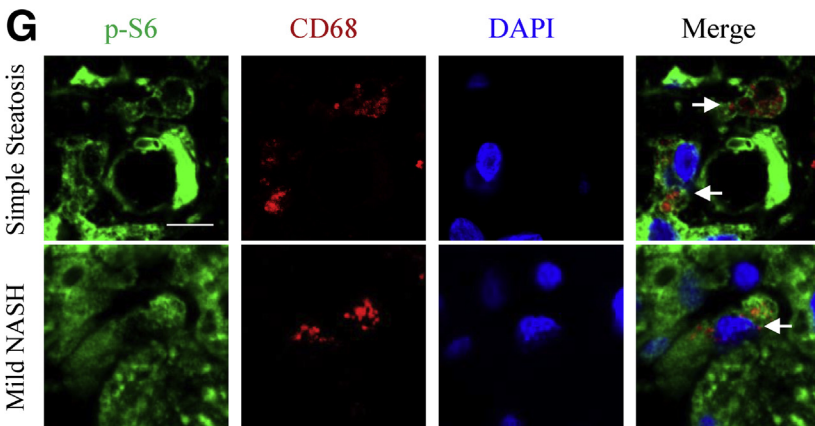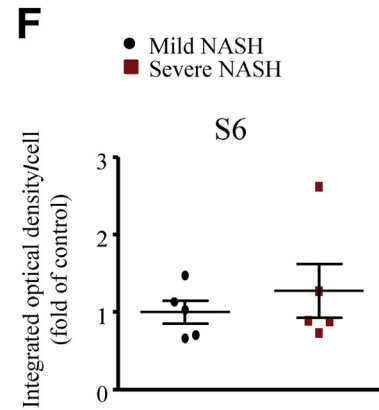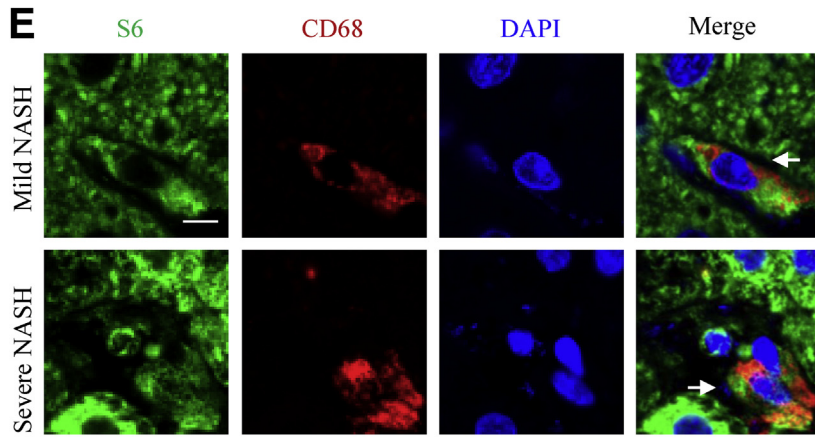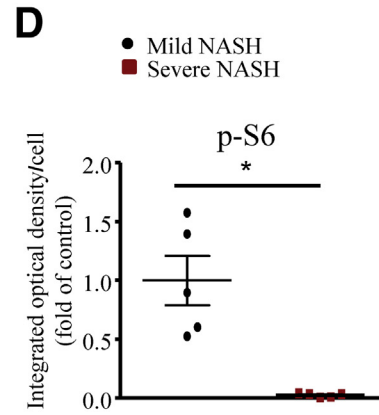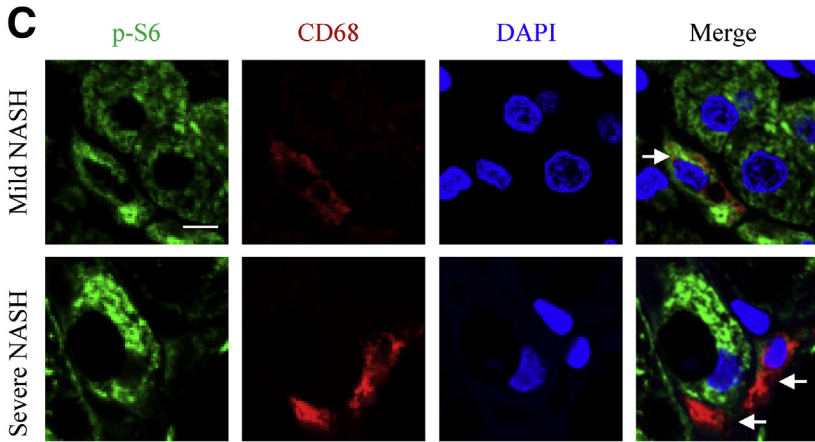
Figure 2. Protein levels of Raptor in peritoneal macrophage from Raptor^{flox} and Raptor^{MacKO} mice. Western blot analysis of protein levels of Raptor in peritoneal macrophage from Raptor^{flox} and Raptor^{MacKO} mice. Similar results were obtained in 3 independent experiments; *horizontal lines* indicate the mean value and *error bars* represent the SEM. *$P < .05$. GAPDH, glyceraldehyde-3-phosphate dehydrogenase.

with macrophages for 30 minutes, or for 6 or 24 hours (Figure 7A). At the beginning of phagocytosis, at 30 minutes, the rate of macrophage engulfment of AHs was measured, but control and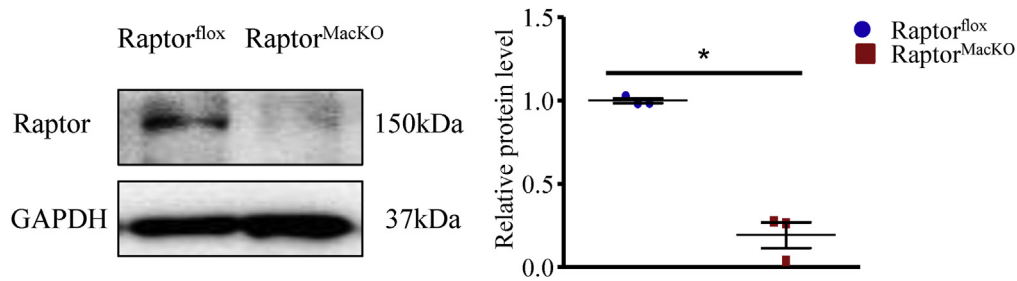 Raptor-deficient macrophages did not differ in phagocytosis rate (Figure 7B and C). After 6 or 24 hours, the engulfed apoptotic cells were degraded and rapidly shrank in size in control macrophages, but more slowly in Raptor-deficient macrophages (Figure 7B).

Lack of mTORC1 Showed Phagolysosome Dysfunction and Defective Lysosome Acidification in Macrophages

During phagocytosis, the maturation of phagolysosomes requires the fusion of phagosomes and lysosomes, which proceeds to the phagolysosome and results in the degradation and reprocessing of the dead cell material.[21] To test whether the impaired AH degradation is caused by phagolysosome dysfunction, we stained the phagolysosome by using LysoTracker in both control and Raptor-deficient macrophages with or without AH incubation. Apoptotic cells with slow shrinkage co-localized with LysoTracker, which indicates possible defective lysosome function in Raptor-deficient macrophages (Figure 8A–C, Supplementary Movies 1 and 2). Moreover, we treated Raptor^{MacKO} and Raptor^{flox} macrophages with apoptotic Jurkat cells. Similar to AH, the degradation of apoptotic Jurkat cells also was impaired in Raptor-deficient macrophages (Figure 8D), which indicates that phagolysosome dysfunction was not AH-specific.

Most of the digestive enzymes present in lysosomes function optimally in an acidic environment; thus, low pH is required for maintaining normal lysosome function. We measured the pH of macrophage lysosomes by using Lyso-Sensor. The pH values were calculated by using a pH calibration curve (Figure 9A). In control macrophages, the lysosome pH value was reduced to 4.56 after incubation with AHs, a pH that would facilitate activation of acid hydrolases and subsequent digestion in the phagolysosome (Figure 9B). In contrast, Raptor-deficient macrophages showed impaired lysosome acidification as compared with control macrophages (Figure 9B). In addition, we measured lysosome consumption by the protein level of lysosomal-associated membrane protein 1 (LAMP1).[22] With AH incubation, the protein levels of LAMP1 were comparable between control and Raptor-deficient macrophages (Figure 9C). Therefore, the phenotype of mTORC1 disruption-induced phagolysosome dysfunction was caused by defective lysosome acidification.

Impaired Phosphorylation of Drp1 at Ser616 Contributing to mTORC1 Disruption-Induced Phagolysosome Dysfunction Depended on Calcium

In lysosomes, the pH gradients are generated and maintained by regulating the activity of a proton-pumping V-ATPase, which couples the metabolic energy of ATP hydrolysis with proton transport into the lysosome lumen. As the main regulator of lysosome acidification, V-ATPase is controlled by cellular calcium content.[23,24] Recent studies have shown that the apoptotic cell–induced enhancement of cytosolic calcium was disturbed by mitochondrial calcium sequestration owing to Drp1 deficiency,[25] whose active site at Ser616 is phosphorylated by mTORC1.[26,27] We hypothesized that mTORC1 might influence lysosome acidification

Figure 1. (*See previous page*). **Alteration of macrophage mTORC1 activity in patients with NASH.** (A) H&E sections of mild and severe NASH human liver sections. *Scale bar*: 100 μm. (B) NAFLD activity scores of human liver samples. (C) Representative immunofluorescence staining of phospho-S6 (p-S6; green) and the macrophage marker CD68 (red) in human liver sections from patients with either mild or severe NASH. *Scale bar*: 6 μm. (D) Quantification of mean integrated optical density of p-S6 in CD68-positive cells. (E) Representative immunofluorescence staining of total S6 (green) and macrophage marker CD68 (red) in human liver sections reflecting mild or severe NASH. *Scale bar*: 6 μm. (F) Quantification of mean integrated optical density of S6 in CD68-positive cells. (A–F) n = 5 in each group. (G) Representative immunofluorescence staining of p-S6 (green) and the macrophage marker CD68 (red) in human liver sections from patients with either simple steatosis or mild NASH. *Scale bar*: 6 μm. (H) Quantification of mean integrated optical density of p-S6 in CD68-positive cells. (G and H) n = 4–5 in each group. *Arrows* indicate liver macrophage; each *point* represents an individual human sample; *horizontal lines* indicate the mean value, and *error bars* represent the SEM. *$P < .05$. DAPI, 4′,6-diamidino-2-phenylindole.
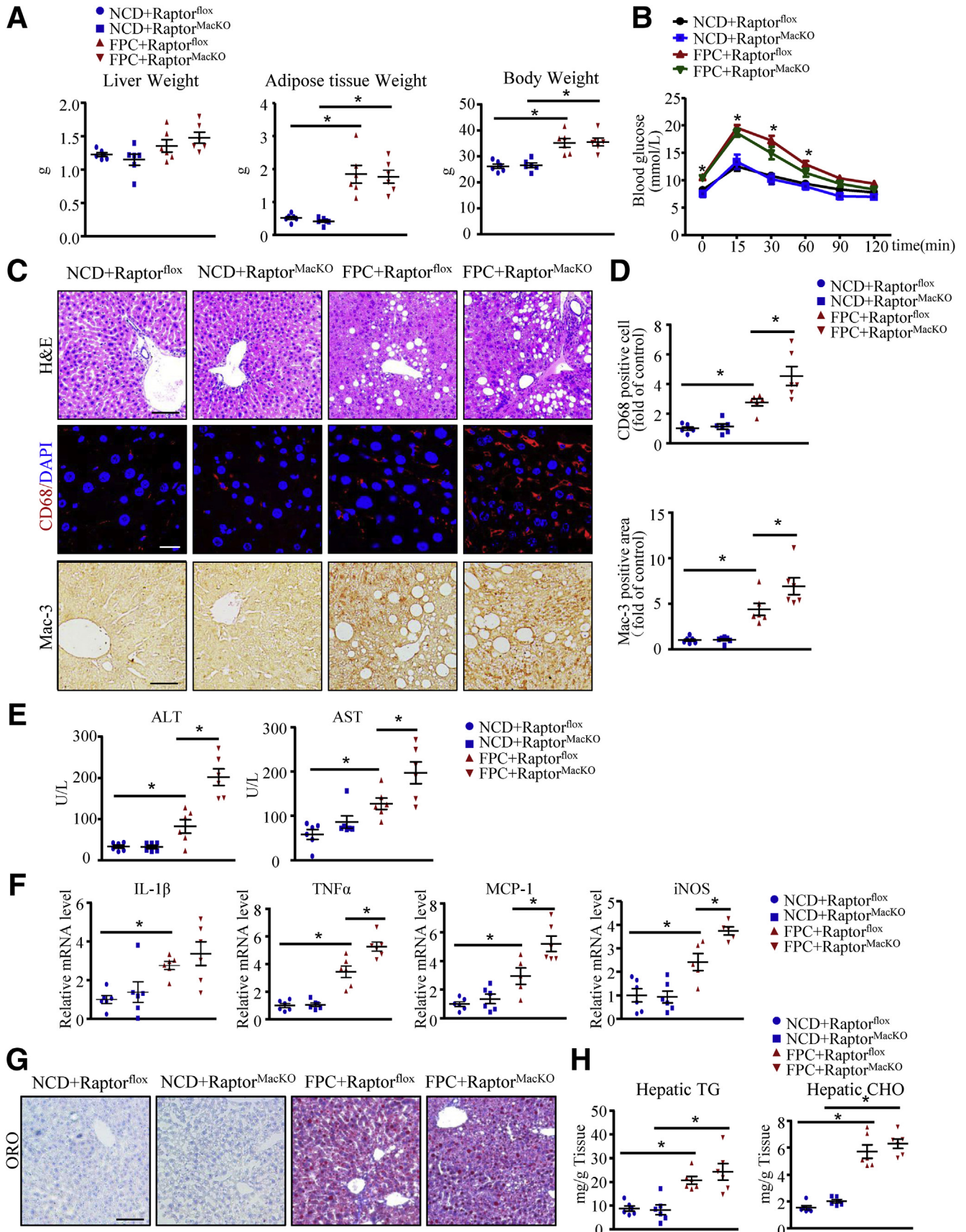
dependent on Drp1 or calcium. To test our hypothesis, we first examined whether Drp1 could be regulated by mTORC1 in macrophages. The co-localization of Drp1 and mTOR was increased in macrophages after treatment with AHs, but was reversed by mTORC1 disruption (Figure 10A). To further determine specific interaction between mTORC1 and Drp1, we co-immunoprecipitated proteins from control and AH–treated macrophages with anti-Drp1 or anti-Raptor antibody. Drp1 specifically bound to the complex mTORC1 in AH-treated macrophages (Figure 10B). In addition, mTORC1 disruption decreased the phosphorylation of Drp1 at Ser616 induced on AH treatment of macrophages, along with phosphorylation of p70S6K, a downstream effector of mTORC1 (Figure 10C).

Consistent with the levels of phosphorylated Drp1 at Ser616, mitochondrial fission was increased in macrophages during the digestion of AHs (Figure 11A), but was inhibited by mTORC1 deficiency along with impaired AH digestion (Figure 11A). In addition, when challenged with AHs, Raptor-deficient macrophages showed increased mitochondrial calcium but decreased cytosolic calcium levels as compared with wild-type macrophages (Figure 11B and C). We then studied whether lysosome acidification impaired by mTORC1 deficiency depends on calcium. To address this, we used the 2 calcium ionophores ionomycin or A23187 to expand the cytosolic calcium pool. In contrast to AH-treated Raptor-deficient macrophages, lysosome pH and glycerol levels in medium were both reversed by adding ionomycin or A23187 (Figure 11D–G). Thus, mTORC1 deficiency-induced lysosome dysfunction might be attributed to the blunted phosphorylation of Drp1 at Ser616 and the resulting reduced cytosolic calcium content.

Inhibition of Guanosine Triphosphatase Activity of Drp1 Led to Impaired Lysosomal Lipolysis and AH-Induced M2-Like Response in Macrophages

To further elucidate whether macrophage Drp1 is critical in lysosome function, we inhibited Drp1 activity in macrophages pharmacologically with Mdivi-1 or genetically with small interfering RNA (si-Drp1). Similar to mTORC1 disruption, Mdivi-1 or si-Drp1 treatment impaired lysosome acidification (Figure 12A–C) and digestion of AH in macrophages (Figure 12D–F). In addition, the AH-enhanced lipolysis (Figure 13A and B) and increased mRNA levels of anti-inflammatory factors (Figure 13C and D) during phagocytosis were abolished by Mdivi-1 or si-Drp1.

Discussion

NASH is a type of NAFLD that is the leading cause of increased liver transplantation in the United States.[3] Abnormal activation of mTOR signaling in hepatocytes has been implicated in various human liver diseases including steatosis and HCC.[28–31] In clinical practice, mTOR inhibitors were used as immunosuppressants to prevent rejection and were considered potential tumor treatments.[32] However, liver damage and increased hepatic inflammation were the main side effects of mTORC1 inhibitors, which mechanistically remains unknown.[32,33] In this study, we found reduced macrophage mTORC1 activity in livers from patients with severe vs mild NASH. Inhibition of mTORC1 activity in macrophages enhanced the inflammatory response in 2 diet-induced NASH mouse models. Our findings provide evidence explaining the protective role of macrophage mTORC1 activation in resolving and limiting hepatic inflammation in NASH and for why its disruption could lead to disease progression.

Macrophages are critical regulators of the inflammatory response to disease that can be switched to distinct phenotypic programs depending on the microenvironment, involving classically activated (M1) and alternatively activated (M2) macrophages.[13] A dynamic shift toward an anti-inflammatory M2 phenotype in hepatic macrophages diminishes the progression of NASH.[34–36] For instance, IL10 produced by M2-like macrophages acts as an anti-inflammatory cytokine, protecting against NASH by ameliorating hepatocyte damage and hepatic inflammation.[35,37] In our study, macrophage Raptor deficiency led to significantly reduced M2-like response and lower production of anti-inflammatory factors (IL10 and IL13) on exposure to AHs. As a consequence of the disrupted resolution of inflammation, our NASH mouse models showed increasing hepatic inflammation.

As a hub, mTORC1 integrates signals regarding extracellular and intracellular energy status and regulates cellular metabolic responses to guide and optimize the inflammatory response.[19] Because of the complexity of the mTORC1 signaling pathway and its cross-talk with other metabolic regulators in response to different stimuli, the role of mTORC1 in regulating macrophage inflammation remains controversial. Recently, some studies showed that both LPS and IL4 were able to stimulate mTORC1 activation in macrophages. However, macrophages deficient in tuberous sclerosis complex 1, an endogenous mTORC1 inhibitor, were hypersensitive to LPS and increased M1 macrophage

Figure 3. (*See previous page*). **Macrophage-specific Raptor deletion exacerbates inflammation in mice after feeding a FPC diet.** Raptor[flox] and Raptor[MacKO] mice were fed the NCD or FPC diet for 24 weeks. (*A*) Liver weight, adipose tissue weight, and body weight of mice were measured, and (*B*) intraperitoneal glucose tolerance test was performed and glucose levels were measured. (*C*) Liver sections from all mice were stained with H&E, CD68, and Mac-3 antibodies for macrophages. Scale bars: 100 μm (*upper panel*); 20 μm (*middle panel*); and 50 μm (*lower panel*). (*D*) Quantification of the number of CD68-positive cells per field (*upper panel*) and morphometric analysis of Mac-3–stained sections (*lower panel*). (*E*) Plasma ALT and AST levels in mice. (*F*) Hepatic mRNA levels of *IL1β*, *TNFα*, *MCP-1*, and *iNOS* were determined by quantitative polymerase chain reaction analysis. (*G*) Oil-red O (ORO) staining of liver showing hepatic lipid accumulation. *Scale bar*: 100 μm. (*H*) Hepatic triglycerides (TG) and cholesterol (CHO) content. n = 5-6 animals per group; each *point* represents an individual animal, *horizontal lines* indicate the mean value, and *error bars* represent the SEM. *$P < .05$. DAPI, 4′,6-diamidino-2-phenylindole.
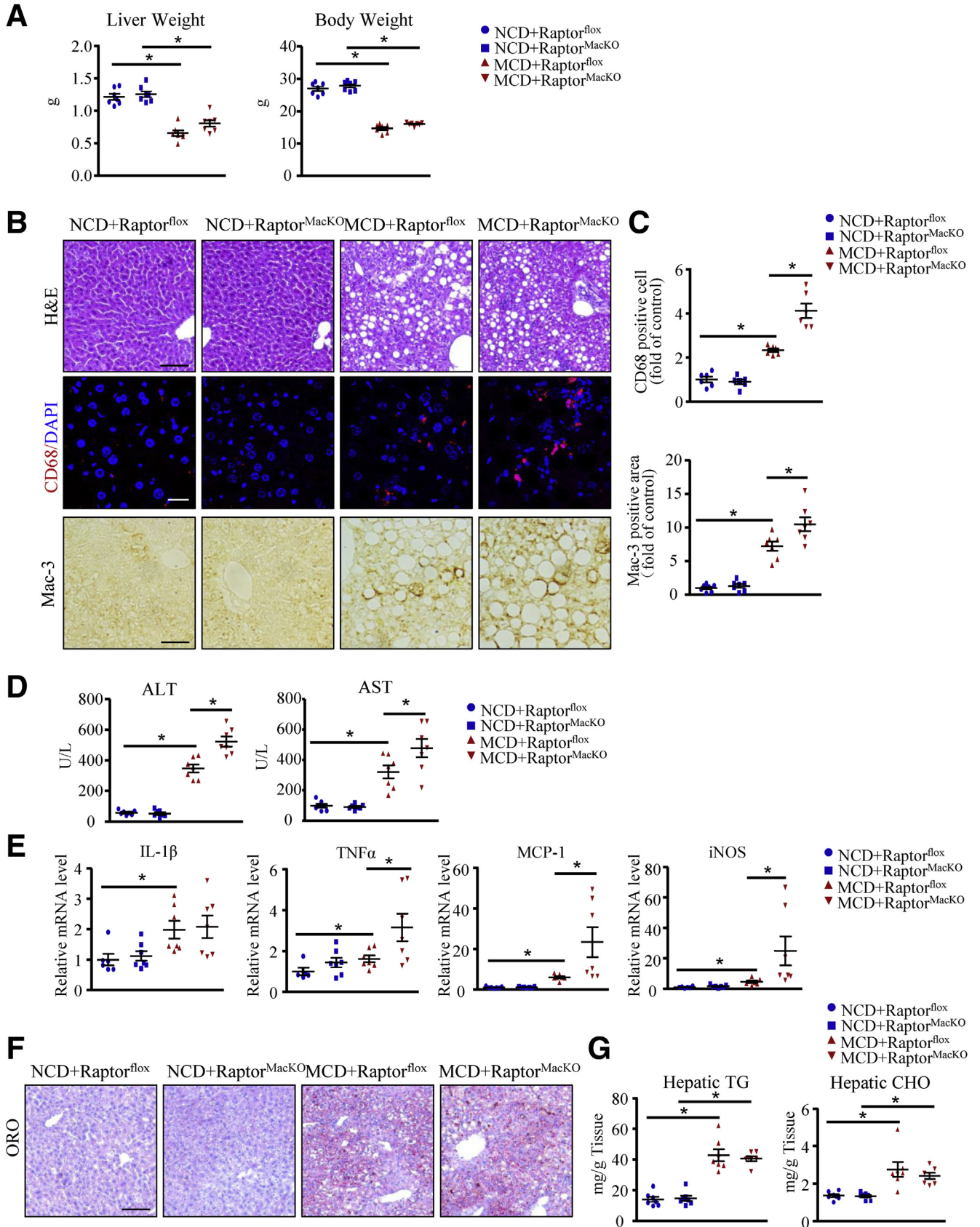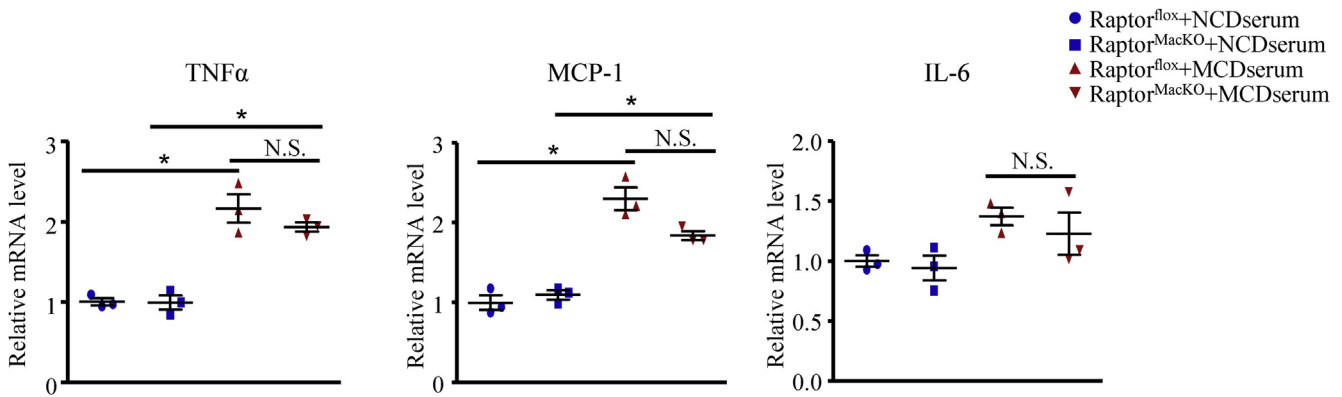
Figure 5. Macrophages from Raptor^flox and Raptor^MacKO mice showed a similar inflammatory response to the MCD serum. Quantitative polymerase chain reaction analysis of mRNA levels of *TNFα*, *MCP-1*, and *IL6* in macrophages obtained from Raptor^flox or Raptor^MacKO mice treated with serum (10%) from mice fed the NCD or MCD diet for 6 hours. Similar results were obtained in 3 independent experiments. *Horizontal lines* indicate the mean value and *error bars* represent the SEM. *$P < .05$.

polarization but showed impaired IL4-induced M2 macrophage polarization.[7,38,39] Paradoxically, similar to our study, Raptor-deficient macrophages showed a defective response to IL4 and reduced expression of M2-specific macrophage genes such as *Retnla* and *Mgl2*.[40] We hypothesized that mTORC1 may have a parabolic relationship with regard to macrophage polarization, with low levels of mTORC1 activity facilitating M2 macrophage gene expression and substantially higher levels of mTORC1 activity, such as in tuberous sclerosis complex 1 deficiency, serving to increase inflammatory gene expression.

Activation of mTORC1 by nutrients and growth factors leads to inhibition of autophagy via the phosphorylation of multiple autophagy-related proteins.[7,41] Intriguingly, impaired autophagy in macrophages caused hepatic inflammation induced by a high-fat diet,[42] which is a similar phenotype as cells with mTORC1 disruption in our NASH models. This divergent observation implied that the phagocytosis-induced anti-inflammatory role of mTORC1 in NASH might be independent of autophagy in macrophages.

Lysosomal pH is regulated mainly by V-ATPase,[43] whose activity is calcium-dependent.[24,44] The cytosolic calcium level was reported to be controlled by dynamic changes of mitochondrial morphology. Fused mitochondria take up calcium from the endoplasmic reticulum, and defective mitochondrial fission can decrease cytosolic calcium level by excessive mitochondrial calcium sequestration.[25,45] Mitochondrial fission is mediated by Drp1, which belongs to the dynamin family of large guanosine triphosphatases.[27]

The phosphorylation of Drp1 at Ser616 promotes, but that at Ser637 inhibits, mitochondrial fission.[27] The phosphorylation of Drp1 at Ser616 during the digestion of AHs was inhibited in Raptor-deficient macrophages, which led to a decreased cytosolic calcium level and impaired lysosome acidification. Consistent with our study, Wang et al[25] showed that Drp1-deficient macrophages failed to show increased cytosolic calcium levels during apoptotic cell internalization.

In addition, our study also showed an important role for cross-talk between mitochondria and lysosomes in cell function. mTORC1 is activated at the lysosomal surface[46] and its binding with Drp1 implies the existence of mitochondria–lysosome contacts. Indeed, consistent with our results, a study performed concurrently by others with our own research observed the mitochondria–lysosome contacts, which mediated the fission of mitochondria and the interaction of mitochondria and lysosomes.[47]

Because we lack an effective tool for gene deletion specifically in liver macrophages, the mouse we used lost Raptor in all macrophages throughout the body. This was a limitation of our study because the macrophages outside the liver also contribute to the progression of NAFLD, especially adipose tissue macrophages. Increased adipose tissue macrophage infiltration is involved in triggering NAFLD by inducing inflammation and insulin resistance.[33] However, our study focused on the stage when the hepatocyte injury-induced wound healing response is critical for the progression of NAFLD.[4] Thus, in our animal models, we emphasized

Figure 4. (See previous page). Macrophage-specific Raptor deletion exacerbates inflammation in mice after feeding a MCD diet. Raptor^flox and Raptor^MacKO mice were fed an NCD or MCD diet for 4 weeks. (*A*) Liver weight and body weight were measured. (*B*) Representative images of H&E staining, immunofluorescence of CD68, and immunohistochemistry of Mac-3 in liver sections from all mice. *Scale bars*: 100 μm (*upper panel*); 20 μm (*middle panel*); and 50 μm (*lower panel*). (*C*) Quantification of the number of CD68-positive cells per field and Mac-3–positive area. (*D*) Plasma ALT and AST levels in mice. (*E*) Hepatic mRNA levels of *IL1β*, *TNFα*, *MCP-1*, and *iNOS* were determined by quantitative polymerase chain reaction analysis. (*F*) Oil-red O (ORO) staining of liver showing hepatic lipid accumulation. *Scale bar*: 100 μm. (*G*) Hepatic triglycerides (TG) and cholesterol (CHO) content. n = 6-7 animals per group. Each *point* represents an individual animal, *horizontal lines* indicate the mean value, and *error bars* represent the SEM. *$P < .05$. DAPI, 4′,6-diamidino-2-phenylindole.

the importance of liver macrophages. Another limitation of our study was that we did not distinguish the role of Kupffer cells and recruited inflammatory monocyte-derived macrophages in Raptor deficiency–induced exacerbated NASH. Liver macrophages include resident macrophages (Kupffer cells) and recruited macrophages.[48] Unlike recruited macrophages, Kupffer cells are stationary. NAFLD can change the liver macrophage proportion.[41] Thus, the role of these macrophages in NAFLD are different. In our study, we used peritoneal macrophages to investigate efferocytosis and the M2-like response, which is widely used to study these functions.[12] However, distinguishing the role of different liver
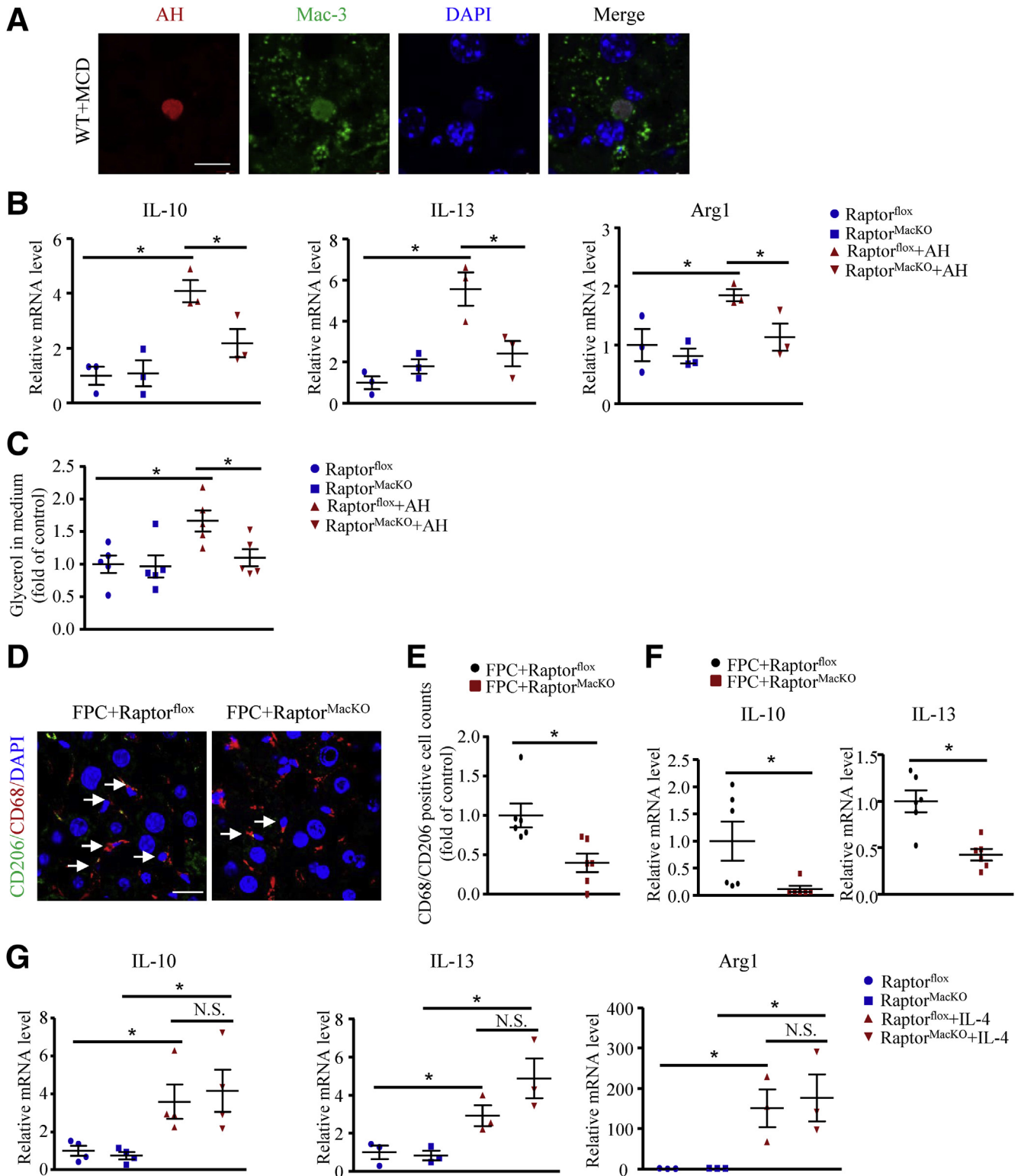
macrophages in this procedure will be more helpful to understand the underlying mechanisms.

Taken together, our data indicate that loss of mTORC1 activity in macrophages promotes hepatic inflammation in both human and rodent NASH. Mechanistic studies suggest that activation of mTORC1 in macrophages is responsible for activating Drp1 and mitochondrial fission to allow for increased cytosolic calcium levels, thereby promoting increased lysosome acidification and lysosomal lipolysis during phagocytosis. As a result, the lipolysis-mediated fatty acid influx promotes M2 macrophage anti-inflammatory factors such as IL10 and IL13 expression. Our findings show that the activation of macrophage mTORC1 in NASH might be a protective process to resolve local inflammation conditions during clearance of apoptotic cells, whereas its disruption leads to more severe liver injury. In addition, our observation might explain why mTORC1 activation by branched-chain amino acids prevents hepatic fibrosis and HCC development in NASH.[49] Our data open up the potential for macrophage mTORC1 as a target for lessening liver inflammation and halting the progression of NASH.

Materials and Methods
Human Liver Specimens

Patients with mild NASH (n = 5) and severe NASH (n = 5) were recruited during scheduling for a liver biopsy for suspected NAFLD from the First Hospital of Tianjin Medical University and Beijing 302 Military Hospital. Liver biopsy specimens were examined by an experienced hepatopathologist with blinding to patient H&E sections. The grades of NASH were classified by the degree of hepatocellular steatosis, ballooning and disarray, and inflammation (intralobular and portal).[50] The study followed the guidelines of the 1975 Declaration of Helsinki and its revisions and was approved by the Research Ethics Committee of Tianjin Medical University. Participants provided informed written consent. No organs were obtained from executed prisoners or other institutionalized persons.

Animals and Treatments

Raptor[flox] mice were crossed with LysMcre mice to generate Raptor[MacKO] and control Raptor[flox] mice (C57BL/6) as described.[7] Age-matched (8 weeks old) male Raptor[MacKO] and Raptor[flox] mice had free access to an FPC diet for 24 weeks[51] or MCD diet (Medicience, Yangzhou, China) for 4 weeks. Control groups of both genotypes were fed a normal chow diet (Medicience). After treatment, mice were killed, and plasma and liver were collected for analysis. All protocols and animal studies were performed in accordance with the Guide for the Care and Use of Laboratory Animals by the US National Institutes of Health (National Institutes of Health publication no. 85-23, updated 2011) and approved by the Institutional Animal Care and Use Committee of Tianjin Medical University (Tianjin, China).

Hepatocyte Isolation

Primary murine hepatocytes were isolated by using collagenase I as described.[52] After attaching for 6 hours, cells were induced to undergo apoptosis by UV radiation.

Peritoneal Macrophage Isolation

To induce accumulation of peritoneal macrophages, the peritoneal cavity was treated with 3% thioglycollate for 3 days. After mice were killed, peritoneal fluid was recovered with 15 mL cold phosphate-buffered saline (PBS). Peritoneal cells were collected by centrifuging at 1500 rpm for 5 minutes and resuspended in Dulbecco's modified Eagle medium containing 10% fetal bovine serum. Nonadherent cells were removed by washing 3 times with warmed PBS after a 2-hour incubation.

Preparation of AHs and Their Engulfment by Macrophages

Primary murine hepatocytes were labeled with Alexa Fluor 488–succinimidyl ester (A20000; Invitrogen/Thermo Fisher Scientific, Waltham, MA) before apoptosis was induced by UV radiation (100 mJ/cm^2, 3 min) as described.[53] After 48 hours, floating AHs were collected. Macrophages were incubated with Dulbecco's modified Eagle medium containing AHs for 30 minutes and 6 and 24 hours. A ratio of approximately 1:1 AHs to macrophages was used in these experiments.

Immunohistochemistry

Paraformaldehyde-fixed and paraffin-embedded livers were cut into 5-μm sections, deparaffinized, rehydrated, and then incubated with anti–Mac-3 antibody (sc-19991; Santa Cruz Biotechnology, Santa Cruz, CA) at 4°C overnight and

Figure 6. (*See previous page*). **AH-induced M2-like response in macrophages was inhibited by Raptor deficiency.** (*A*) AHs engulfed by macrophages in liver detected by immunofluorescence staining of Mac-3 (green) and terminal deoxynucleotidyl transferase–mediated deoxyuridine triphosphate nick-end labeling staining (red). Nuclei were counterstained with 4′,6-diamidino-2-phenylindole (DAPI) (blue). *Scale bar*: 10 μm. n = 5 animals per group, and a representative result is shown. (*B* and *C*) Macrophages from Raptor[flox] and Raptor[MacKO] mice were treated with or without AHs for 6 hours. (*B*) Quantitative polymerase chain reaction analysis of mRNA levels of *IL10*, *IL13*, and *arginase-1 (Arg1)*; similar results were obtained in 3 independent experiments. (*C*) Relative fold change of glycerol level in macrophage medium; similar results were obtained in 5 independent experiments. (*D–F*) Raptor[flox] and Raptor[MacKO] mice were fed the FPC diet for 24 weeks. (*D*) Immunofluorescence staining of CD206 (green) and CD68 (red) in liver sections of FPC-treated Raptor[flox] and Raptor[MacKO] mice (*scale bar*: 20 μm) and (*E*) quantification of CD68/206-positive cells per field. (*F*) Quantitative polymerase chain reaction analysis of hepatic mRNA levels of *IL1* and *IL13* in FPC-treated Raptor[flox] and Raptor[MacKO] mice. n = 6 animals per group. Each *point* represents an individual animal. (*G*) Quantitative polymerase chain reaction analysis of mRNA levels of *IL10*, *IL13*, and *Arg1* in macrophages from Raptor[flox] or Raptor[MacKO] mice treated with IL4 (20 ng/mL) for 6 hours; similar results were obtained in 3–4 independent experiments. *Horizontal lines* indicate the mean value and *error bars* represent the SEM. *$P < .05$. WT, wild-type.
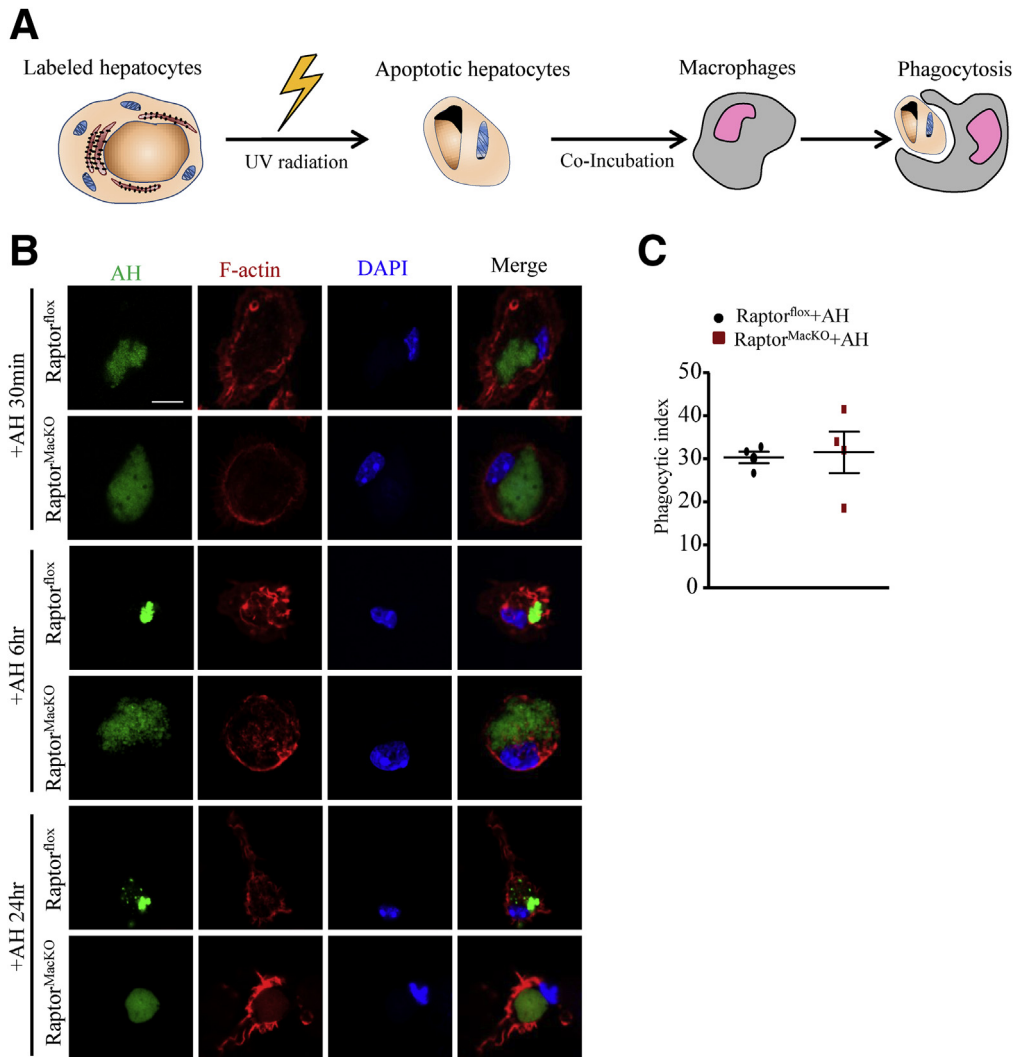
A

B

C

Figure 7. Macrophages from Raptor^{MacKO} mice showed a deficiency in digesting AHs. Primary hepatocytes were labeled with succinimidyl ester (green) for 30 minutes before treatment with UV to induce apoptosis. Macrophages from Raptor^{flox} and Raptor^{MacKO} mice were treated with AH for the indicated time. (*A*) Schematic representation of the digestion method. (*B*) Macrophages from Raptor^{flox} and Raptor^{MacKO} mice were treated with AHs as shown in panel *A* for 30 minutes or 6 or 24 hours. F-actin (red) was used to label the cytoskeleton. (*C*) Phagocytic index calculated at 30 minutes. Similar results were obtained in 4 independent experiments; a representative result is shown. *horizontal lines* indicate the mean value and *error bars* represent the SEM. DAPI, 4′,6-diamidino-2-phenylindole.

with secondary antibody for 30 minutes. The reaction was developed with diaminobenzidine staining.

Immunofluorescence Staining and Confocal Microscopy

Human liver sections were incubated with anti–p-S6 (5364; Cell Signaling Technology, Danvers, MA) or S6 (2217; Cell Signaling Technology) antibodies, and mouse liver sections were stained with CD68 (ab955; Abcam, Cambridge, MA) or CD206 antibody (ab64693; Abcam) at 4°C overnight. Sections were incubated with secondary antibodies for 30 minutes. Images were acquired using a Leica (Buffalo Grove, IL) confocal microscope. Five fields of each sample were used to quantify the confocal images.

For evaluating the phagocytic index, macrophages were incubated with AHs labeled with Alexa Fluor 488–succinimidyl ester (A20000; Invitrogen/Thermo Fisher Scientific) for 30 minutes, washed 3 times, and stained with F-actin (DyLight 554 phalloidin, 13054; Cell Signaling

Technology). The number of macrophages engulfing AHs was divided by the total number of macrophages in at least 4 fields to calculate the phagocytosis index. Images were acquired by confocal microscopy with 40× magnification.

For lysosome or mitochondria labeling, cells were stained with LysoTracker Red DND-99 (L7528; Invitrogen/Thermo Fisher Scientific, Waltham, MA) for 30 minutes or MitoTracker (M75125; Invitrogen/Thermo Fisher Scientific) for 15 minutes at 37°C following the manufacturer's protocol. Macrophage lysosomes in live cells were labeled, and AHs were stained with Alexa Fluor 488–succinimidyl ester (A20000; Invitrogen/ Thermo Fisher Scientific). The labeled AHs were added into the medium of macrophages. Images were taken starting from 0 hours, then every 15 minutes for 6 hours under an Olympus (Shinjuku-ku, Tokyo) confocal microscope.

For immunofluorescence staining of macrophages, cells were labeled with an antibody against Drp1 (8570; Cell Signaling Technology), mTOR (ab87540; Abcam), or LAMP1 (ab24170; Abcam) overnight at 4°C, then with Alexa Fluor 594 or 488 antibodies (1:200) for 1 hour. The number of

A

B

C

D

Figure 8. Macrophages from Raptor^MacKO mice showed phagolysosome dysfunction. (*A*) Lyso-Tracker (red) was used to label lysosomes after macrophages were treated with SE-labeled AH (green) for 6 hours. Representative LysoTracker, succinimidyl easter (SE), and merge images are shown. *Scale bar*: 10 μm. Similar results were obtained in 5 independent experiments. (*B*) AHs were labeled with SE (green), and lysosomes were labeled with LysoTracker (red). Live images of AH digestion (*arrows*) in lysosomes were taken every 15 minutes for 6 hours. Also see Supplementary Movies 1 and 2. (*C*) The quantification of the size of engulfed AHs by macrophages in the Supplementary Movies 1 and 2. (*B* and *C*) Similar results were obtained in 3 independent experiments; a representative result is shown. (*D*) LysoTracker (red) was used to label lysosomes after macrophages were treated with succinimidyl ester–labeled apoptotic Jurkat cells (AC) (green) for 6 hours. Representative LysoTracker, AC, and merge images are shown. *Scale bar*: 10 μm. Similar results were obtained in 3 independent experiments; a representative result is shown.
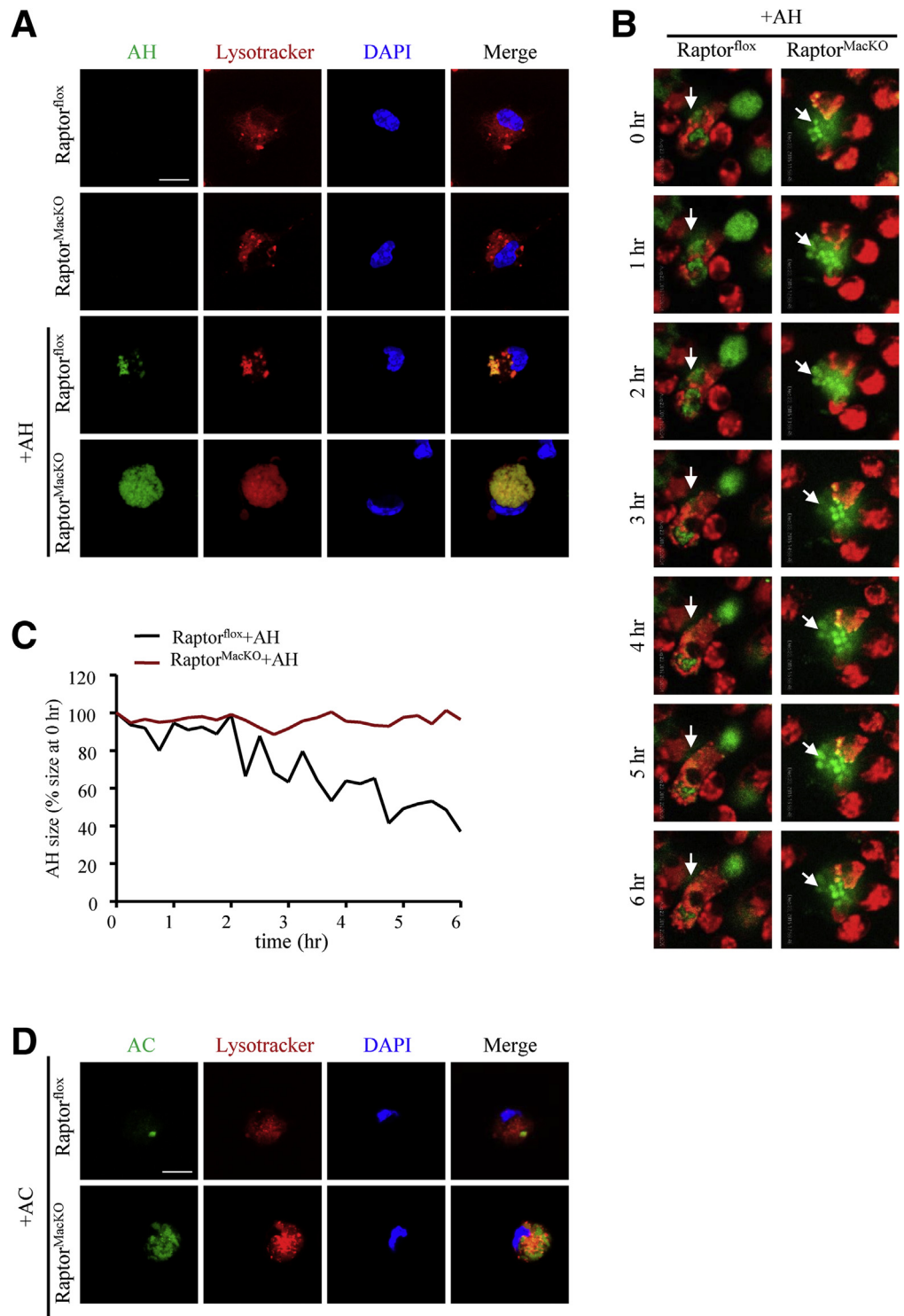
cells was determined by 4′,6-diamidino-2-phenylindole staining. Images were acquired under a Leica confocal microscope.

Lysosomal pH Measurement

LysoSensor Yellow/Blue DND-160 (L7545; Invitrogen/Thermo Fisher Scientific) was used for pH measurement of lysosomes. Cells were labeled with 3 μmol/L LysoSensor Yellow/Blue DND-160 in medium for 5 minutes at 37°C, washed twice with PBS, and immediately analyzed by using a microplate reader (excitation, 360 nm; emission, 451 and 518 nm). Quantification of lysosomal pH involved a ratio (emission 451/emission 518) according to pH calibration.
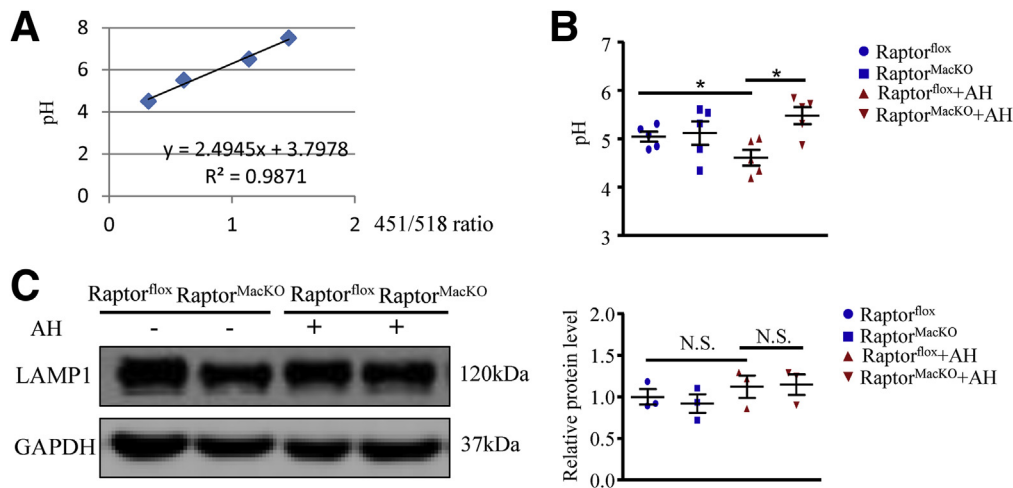
Figure 9. The acidification of lysosomes was impaired in macrophages from Raptor^MacKO mice. (*A*) pH calibration curve. (*B*) Macrophages from Raptor^flox and Raptor^MacKO mice were incubated with or without AHs for 6 hours and then labeled with a pH-sensitive fluorophore LysoSensor. pH values were calculated by pH calibration. Similar results were obtained in 5 independent experiments. (*C*) Western blot analysis of protein levels of LAMP1 in control and Raptor-deficient macrophages treated with or without AHs for 6 hours, and quantification. Glyceraldehyde-3-phosphate dehydrogenase (GAPDH) was an internal control; similar results were obtained in 3 independent experiments. *Horizontal lines* indicate the mean value and *error bars* represent the SEM. *$P < .05$.

The protocol of LysoSensor pH calibration measurement was adapted from the manufacturer's instructions.

Quantitative Polymerase Chain Reaction and Western Blot Analysis

Total RNA from frozen livers or peritoneal macrophages was isolated by using RNA extraction kits (Qiagen, Hilden, Germany) and subjected to complementary DNA synthesis by reverse-transcription with random primers. The mRNA expression of different genes was normalized to that of β-actin. The quantitative polymerase chain reaction procedure followed the Minimum Information for Publication of Quantitative Real-Time Polymerase Chain Reaction Experiments guidelines. Sequences of primers for quantitative polymerase chain reaction are shown in Table 1.

Macrophage protein was extracted and separated by 10% or 12% sodium dodecyl sulfate–polyacrylamide gel electrophoresis and transferred onto polyvinylidene difluoride membranes, which were immunostained with corresponding primary antibodies at 4°C overnight.

siRNA

To knockdown Drp1 in macrophages, a mixture of 3 sets of siRNA against mouse Drp1 was synthesized (Sangon Biotech, Shanghai, China). The sequences were as follows: sense 1, 5'-GCAGAGGAUCAUUCAGCAUUTT-3'; antisense 1, 5'-AUGCUGAAUGAUCCUCUGCUT-3'; sense 2, 5'-GCUACUU UACUCCAGCUUAUTT-3'; antisense 2, 5'-UAAGCUGGAGU AAAGUAGCUT-3'; and sense 3, 5'-GCAGAACUCUAGCUGUA AUTT-3'; antisense 3, 5'-AUUACAGCUAGAGUUCUGCUT-3'.

Determination of Plasma ALT/AST Levels

ALT and AST plasma levels in mice were analyzed by the Tianjin Medical University Metabolic Diseases Hospital.

| Table 1. List of Oligonucleotide Primer Pairs Used in Quantitative Polymerase Chain Reaction		
Target gene	Sense primer	Antisense primer
iNOS	5'-CCCCGCTACTACTCCATCAG-3'	5'-CCACTGACACTTCGCACAAA-3'
TNFα	5'-CCAGACCCTCACACTCAGATC-3'	5'-CACTTGGTGGTTTGCTACGAC-3'
IL1β	5'-GCCCATCCTCTGTGACTCAT-3'	5'-AGGCCACAGGTATTTTGTCG-3'
IL6	5'-ACAACCACGGCCTTCCCTACTT-3'	5'-CACGATTTCCCAGAGAACATGTG-3'
MCP-1	5'-AGCCAACTCTCACTGAAGCCA-3'	5'-TCTGGACCCATTCCTTCTTGG-3'
IL10	5'-TAAGGGTTACTTGGGTTGC-3'	5'-GAGGGTCTTCAGCTTCTCAC-3'
IL13	5'-GTCCTGGCTCTTGCTTGCC-3'	5'-CCATACCATGCTGCCGTTG-3'
Arginase-1	5'-CTGAGCTTTGATGTCGACGG-3'	5'-TCCTCTGCTGTCTTCCCAAG-3'
β-actin	5'-CTGTCCCTGTATGCCTCT-3'	5'- ATGTCACGCACGATTTCC-3'
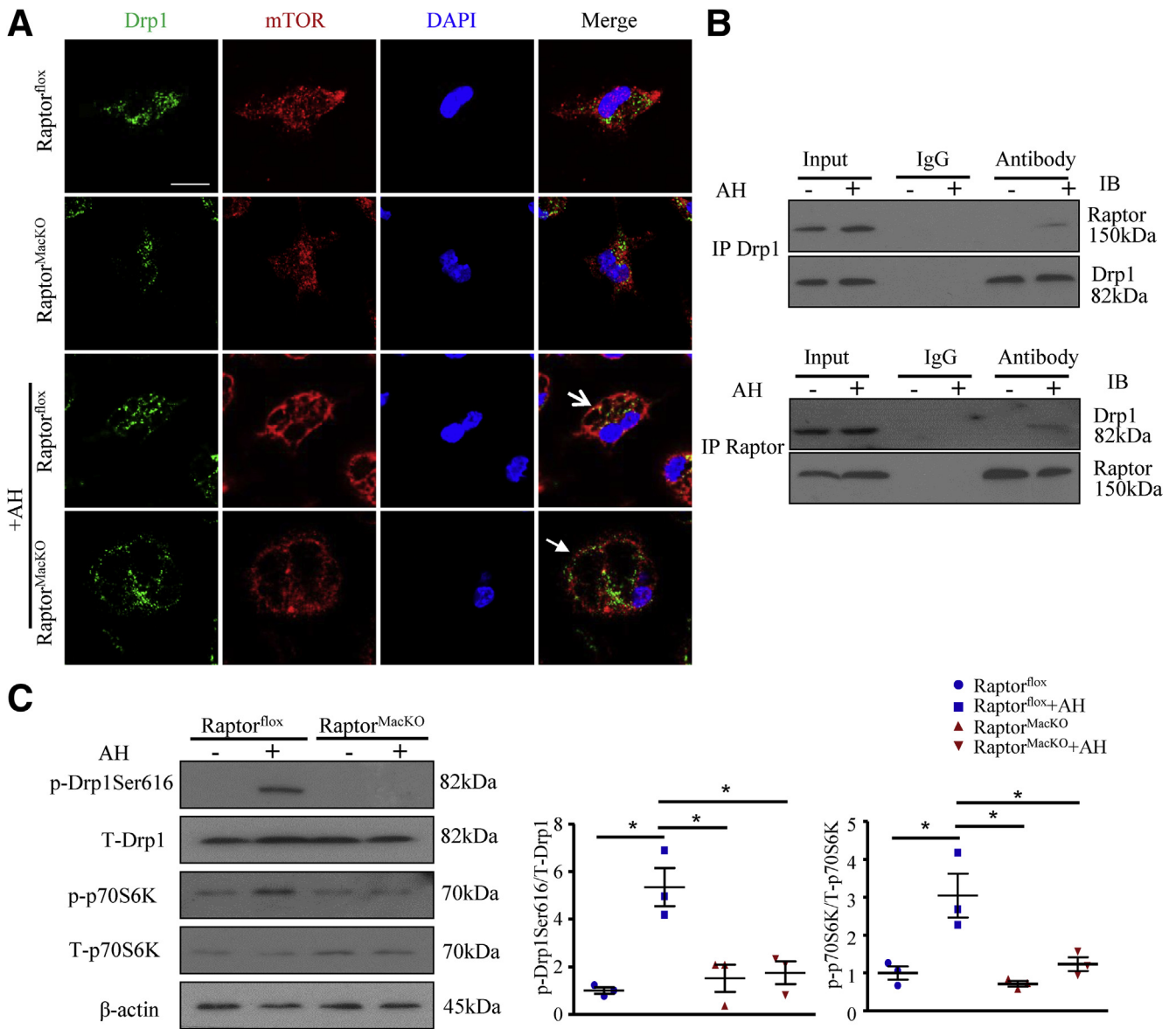
Figure 10. Lack of mTORC1 inhibited Drp1 activation. Macrophages were incubated with or without AHs for 6 hours. (*A*) Immunofluorescence staining of the co-localization of Drp1 (green) and mTOR (red). *Scale bar*: 10 μm. Similar results were obtained from 5 independent experiments; a representative result is shown. (*B*) Immunoprecipitation (IP) of Drp1 and Raptor, and Western blot analysis (IB) of Drp1 and Raptor protein level. (*C*) Western blot analysis of protein levels of p-Drp1 (Ser616), total Drp1, p-p70S6K, and total p70S6K and quantification; β-actin was an internal control. Similar results were obtained in 3 independent experiments. *Horizontal lines* indicate the mean value and *error bars* represent the SEM. *$P < .05$. DAPI, 4′,6-diamidino-2-phenylindole; IB, immunoblotting; IP, Immunoprecipitates.

Determination of Hepatic Triglycerides and Cholesterol Content

Approximately 50 mg of liver tissue was homogenized at 4°C in 1 mL chloroform-methanol extraction buffer (2:1). Samples were neutralized with 300 μL deionized water. After centrifugation (12,000 rpm, 10 min), the supernatant was collected and dried under nitrogen. After solubilizing the samples in 200 μL 5% Triton X-100 (Solarbio Inc, Beijing, China) in water, the triglyceride or cholesterol quantity was determined by using a triglyceride or cholesterol determination kit (BioSino Bio-Technology and Science, Beijing, China) as the manufacturer instructed.

Determination of Glycerol Level in Medium

The glycerol level in macrophage medium was determined by using a glycerol assay kit (E1002; Applygen Technologies, Inc, Beijing, China) as the manufacturer instructed.

Analysis of Cytosolic and Mitochondrial Calcium Levels

For cytosolic or mitochondrial calcium measurements, macrophages were treated with AHs for 6 hours, and then cells were loaded with 8 μmol/L Fluo-4-AM (F312; Dojindo
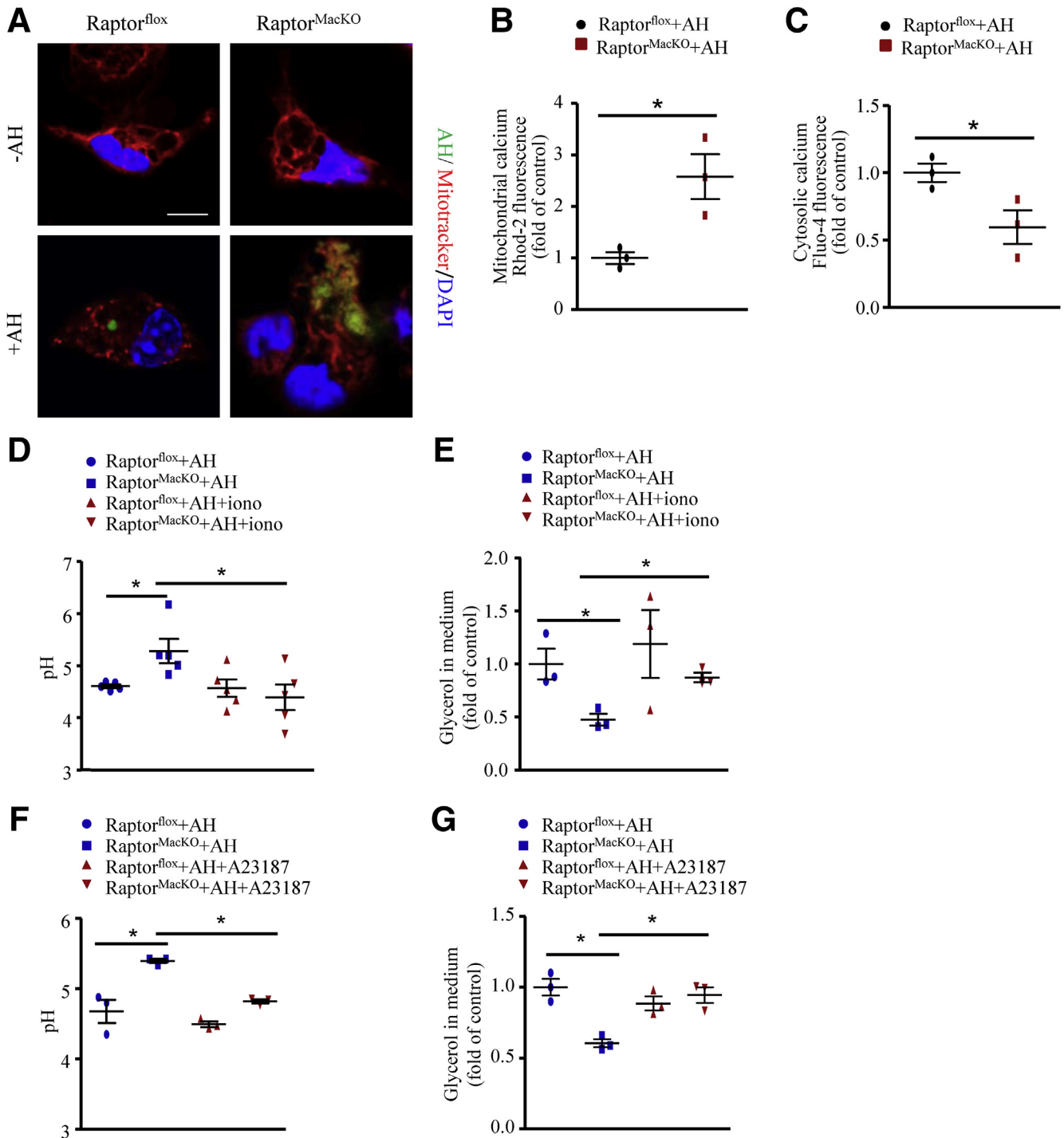
Figure 11. Lack of mTORC1 inhibited mitochondrial fission, decreased cytosolic calcium level, and subsequently inhibited lysosome acidification in macrophages. (*A*) Macrophages were incubated with succinimidyl easter (SE)-labeled AH (green) for 6 hours, and MitoTracker (red) was used to label mitochondria. *Scale bar*: 10 μm. Similar results were obtained in 3 independent experiments; a representative result is shown. (*B* and *C*) Macrophages were incubated with AHs for 6 hours. The relative mitochondrial and cytosolic calcium levels were analyzed by (*B*) Rhod-2-AM and (*C*) Fluo-4-AM, respectively. Similar results were obtained in 3 independent experiments. (*D* and *E*) Control and Raptor-deficient macrophages were treated with AHs for 6 hours with or without ionomycin (2 μmol/L). (*D*) A pH-sensitive fluorophore LysoSensor was added and pH values were calculated by pH calibration. Similar results were obtained in 5 independent experiments. (*E*) Relative fold change of glycerol level in medium; similar results were obtained in 3 independent experiments. (*F* and *G*) Control and Raptor-deficient macrophages were treated with AHs for 6 hours with or without A23187 (1 μmol/L). (*F*) pH values were calculated. (*G*) Relative fold change of glycerol level in medium. similar results were obtained in 3 independent experiments. *Horizontal lines* indicate the mean value and *error bars* represent the SEM. *$P < .05$. DAPI, 4′,6-diamidino-2-phenylindole.
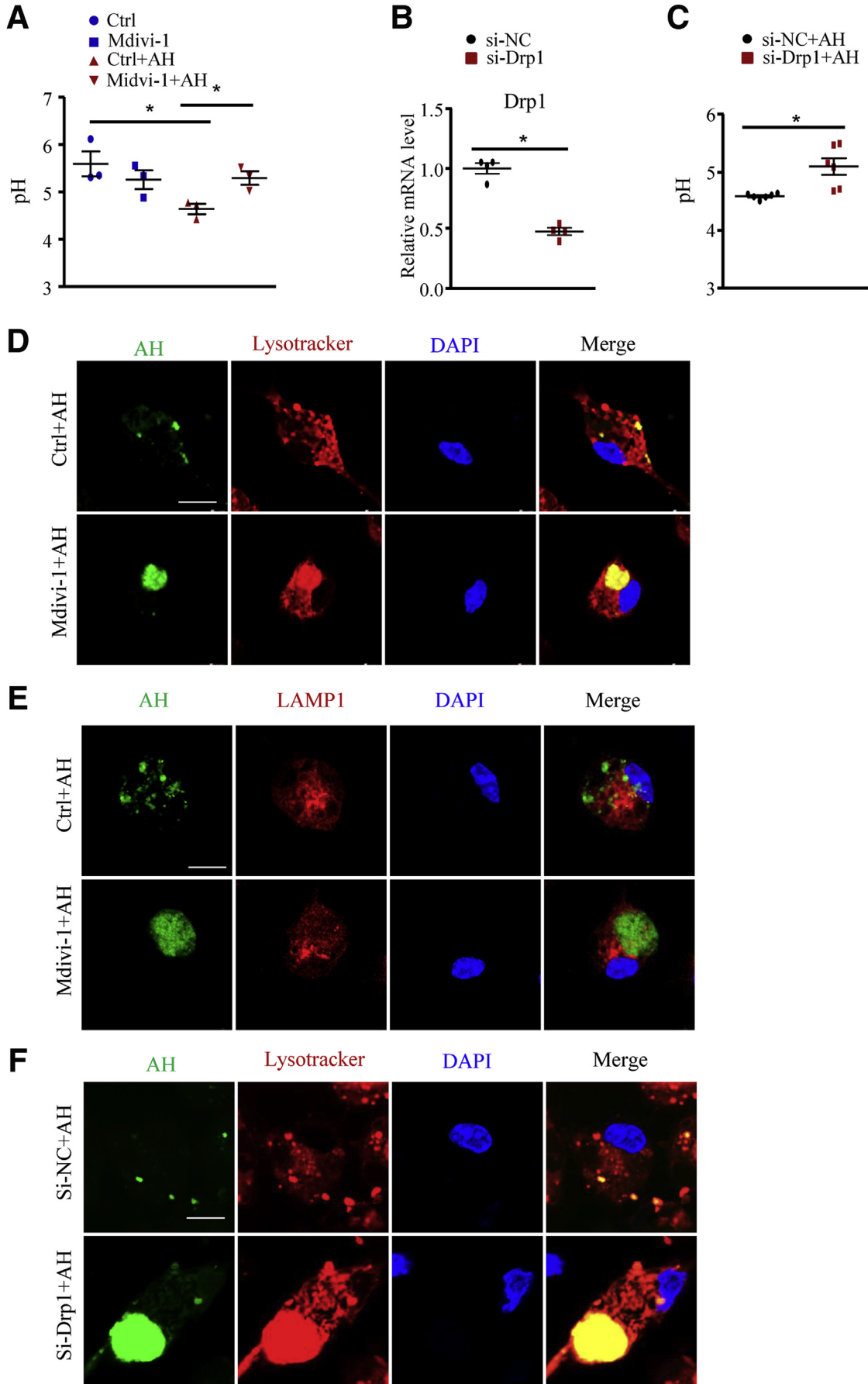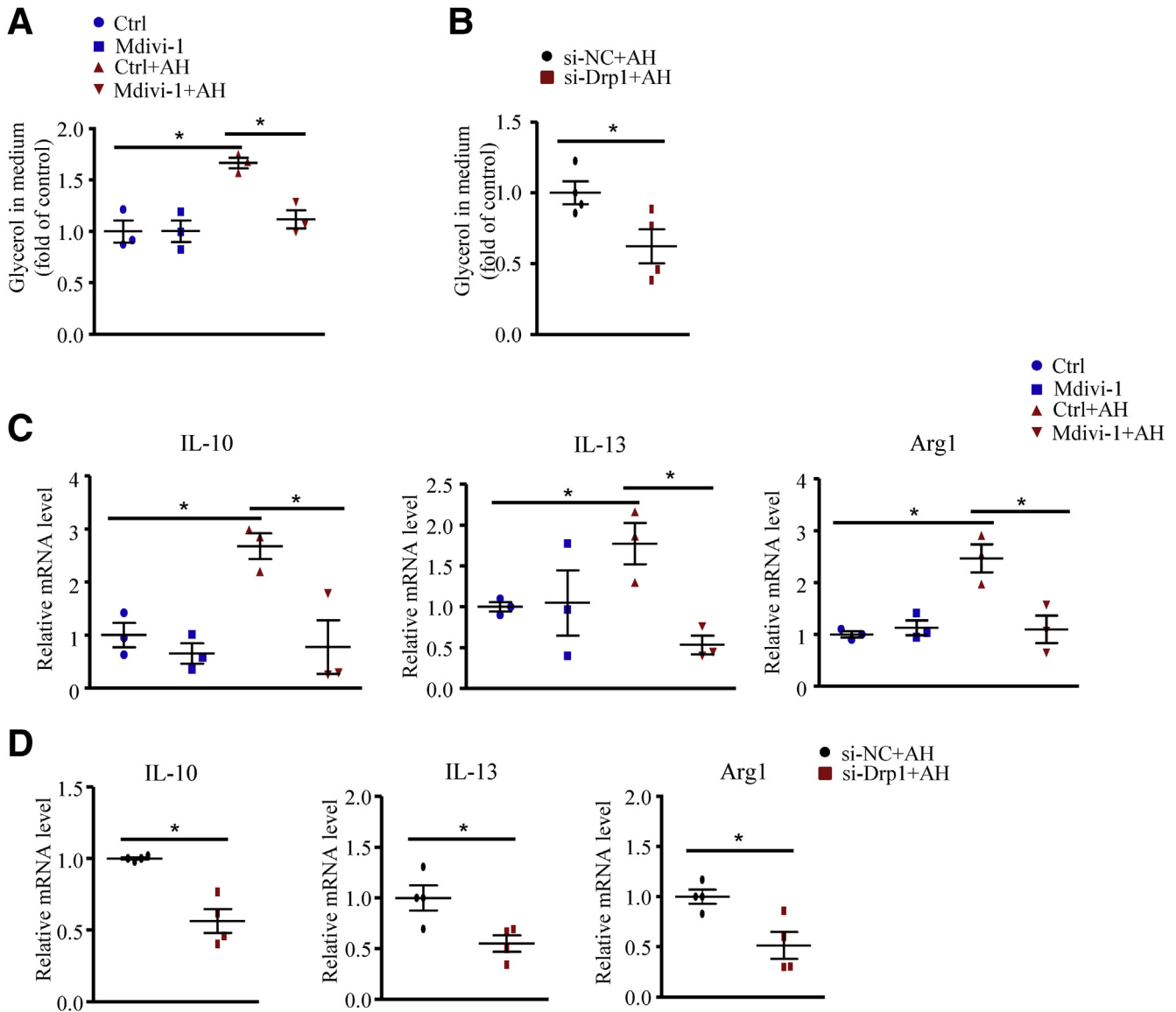
Figure 13. Drp1 inhibition impaired lysosome-mediated lipolysis and M2-like responses induced by apoptotic hepatocytes. Macrophages were pretreated with the Drp1 inhibitor Mdivi-1 (25 μmol/L) for 24 hours or transfected with si-Drp1 for 48 hours, then incubated with or without AHs for 6 hours. (*A* and *B*) Relative fold change of glycerol level in medium. (*C* and *D*) Quantitative polymerase chain reaction analysis of mRNA levels of IL10, IL13, and arginase-1 (Arg1). Similar results were obtained in 3–4 independent experiments. *Horizontal lines* indicate the mean value and *error bars* represent the SEM. *$P < .05$. NC, negative control.

Figure 12. (*See previous page*). Drp1 inhibition impaired lysosome acidification induced by apoptotic hepatocytes. Macrophages were pretreated with the Drp1 inhibitor Mdivi-1 (25 μmol/L) for 24 hours or transfected with si-Drp1 for 48 hours, then incubated with or without AHs for 6 hours. (*A*) Macrophages treated with Mdivi-1 were labeled with LysoSensor, and pH values were calculated by pH calibration. Similar results were obtained in 3 independent experiments. (*B*) Quantitative polymerase chain reaction analysis of mRNA levels of Drp1. Similar results were obtained in 4 independent experiments. (*C*) Macrophages transfected with si-NC (scramble siRNA) or si-Drp1 were labeled with LysoSensor, and pH values were calculated by pH calibration. Similar results were obtained in 3 independent experiments. (*D* and *E*) Representative images of macrophages treated with Mdivi-1; lysosomes were labeled with (*D*) LysoTracker (red) or (*E*) LAMP1 (red), and AHs were labeled with SE (green). *Scale bar*: 10 μm. Similar results were obtained in 3 independent experiments. A representative result is shown. (*F*) Representative images of macrophages transfected with si-NC or si-Drp1; lysosomes were labeled with LysoTracker (red) and AHs were labeled with SE (green). *Scale bar*: 10 μm. Similar results were obtained in 3 independent experiments. A representative result is shown. *Horizontal lines* indicate the mean value and *error bars* represent the SEM. *$P < .05$. DAPI, 4′,6-diamidino-2-phenylindole; NC, negative control.

Laboratories, Kumamoto, Japan) or Rhod-2-AM (R001; Dojindo Laboratories) for 30 minutes in the dark as the manufacturer instructed, respectively.[54] After being washed for 3 times and incubated with Hank's balanced salt solution or HEPES buffer saline for 30 minutes, cells were analyzed on an Olympus confocal microscope. The relative cytosolic and mitochondrial levels were calculated by the fluorescence intensity per cell.

Immunoprecipitates

Macrophage protein was precleared by using protein A/G agarose beads at 4°C for 1 hour on a rotator. After centrifugation, anti-Drp1 or anti-Raptor antibody (4978; Cell Signaling Technology) or IgG was added into the supernatant 2 hours before protein A/G agarose beads were added and incubated at 4°C overnight on a rotator. Then, beads were washed 3 times and protein was dissociated from beads by protein loading buffer containing sodium dodecyl sulfate at 100°C for 5 minutes.

Statistical Analysis

All data are presented as means ± SEM and were analyzed by an unpaired *t* test or 1-way analysis of variance for comparing more than 2 groups. $P < .05$ was considered statistically significant. Statistical analysis involved use of GraphPad Prism v5.01 (GraphPad Software, San Diego, CA).

All authors had access to the study data and reviewed and approved the final manuscript.

References

1. Ahmed M. Non-alcoholic fatty liver disease in 2015. World J Hepatol 2015;7:1450–1459.
2. Henao-Mejia J, Elinav E, Jin C, Hao L, Mehal WZ, Strowig T, Thaiss CA, Kau AL, Eisenbarth SC, Jurczak MJ, Camporez JP, Shulman GI, Gordon JI, Hoffman HM, Flavell RA. Inflammasome-mediated dysbiosis regulates progression of NAFLD and obesity. Nature 2012;482:179–185.
3. Wong RJ, Cheung R, Ahmed A. Nonalcoholic steatohepatitis is the most rapidly growing indication for liver transplantation in patients with hepatocellular carcinoma in the U.S. Hepatology 2014;59:2188–2195.
4. Diehl AM, Day C. Cause, pathogenesis, and treatment of nonalcoholic steatohepatitis. N Engl J Med 2017; 377:2063–2072.
5. Ratziu V, Goodman Z, Sanyal A. Current efforts and trends in the treatment of NASH. J Hepatol 2015; 62:S65–S75.
6. Haissaguerre M, Saucisse N, Cota D. Influence of mTOR in energy and metabolic homeostasis. Mol Cell Endocrinol 2014;397:67–77.
7. Ai D, Jiang H, Westerterp M, Murphy AJ, Wang M, Ganda A, Abramowicz S, Welch C, Almazan F, Zhu Y, Miller YI, Tall AR. Disruption of mammalian target of rapamycin complex 1 in macrophages decreases chemokine gene expression and atherosclerosis. Circ Res 2014;114:1576–1584.
8. Wang L, Luo JY, Li B, Tian XY, Chen LJ, Huang Y, Liu J, Deng D, Lau CW, Wan S, Ai D, Mak KK, Tong KK, Kwan KM, Wang N, Chiu JJ, Zhu Y, Huang Y. Integrin-YAP/TAZ-JNK cascade mediates atheroprotective effect of unidirectional shear flow. Nature 2016;540:579–582.
9. Yilmaz Y. Review article: is non-alcoholic fatty liver disease a spectrum, or are steatosis and non-alcoholic steatohepatitis distinct conditions? Aliment Pharmacol Ther 2012;36:815–823.
10. Tosello-Trampont AC, Landes SG, Nguyen V, Novobrantseva TI, Hahn YS. Kuppfer cells trigger nonalcoholic steatohepatitis development in diet-induced mouse model through tumor necrosis factor-alpha production. J Biol Chem 2012;287:40161–40172.
11. Ju C, Tacke F. Hepatic macrophages in homeostasis and liver diseases: from pathogenesis to novel therapeutic strategies. Cell Mol Immunol 2016;13:316–327.
12. Huang SC, Everts B, Ivanova Y, Huang SC, Everts B, Ivanova Y, O'Sullivan D, Nascimento M, Smith AM, Beatty W, Love-Gregory L, Lam WY, O'Neill CM, Yan C, Du H, Abumrad NA, Urban JF Jr, Artyomov MN, Pearce EL, Pearce EJ. Cell-intrinsic lysosomal lipolysis is essential for alternative activation of macrophages. Nat Immunol 2014;15:846–855.
13. Heckmann BL, Boada-Romero E, Cunha LD, Magne J, Green DR. LC3-associated phagocytosis and inflammation. J Mol Biol 2017;429:3561–3576.
14. Odegaard JI, Chawla A. Alternative macrophage activation and metabolism. Annu Rev Pathol 2011;6:275–297.
15. Sharma M, Mitnala S, Vishnubhotla RK, Mukherjee R, Reddy DN, Rao PN. The riddle of nonalcoholic fatty liver disease: progression from nonalcoholic fatty liver to nonalcoholic steatohepatitis. J Clin Exp Hepatol 2015; 5:147–158.
16. Rinella ME, Siddiqui MS, Gardikiotes K, Gottstein J, Elias M, Green RM. Dysregulation of the unfolded protein response in db/db mice with diet-induced steatohepatitis. Hepatology 2011;54:1600–1609.
17. Marra F, Lotersztajn S. Pathophysiology of NASH: perspectives for a targeted treatment. Curr Pharm Des 2013; 19:5250–5269.
18. Wattacheril J, Issa D, Sanyal A. Nonalcoholic steatohepatitis (NASH) and Hepatic fibrosis: emerging therapies. Annu Rev Pharmacol Toxicol 2018;58:649–662.
19. Hirsova P, Gores GJ. Death receptor-mediated cell death and proinflammatory signaling in nonalcoholic steatohepatitis. Cell Mol Gastroenterol Hepatol 2015;1:17–27.
20. Brenner C, Galluzzi L, Kepp O, et al. Decoding cell death signals in liver inflammation. J Hepatol 2013;59:583–594.
21. Elliott MR, Ravichandran KS. Clearance of apoptotic cells: implications in health and disease. J Cell Biol 2010; 189:1059–1070.
22. Ma X, Godar RJ, Liu H, Diwan A. Enhancing lysosome biogenesis attenuates BNIP3-induced cardiomyocyte death. Autophagy 2012;8:297–309.
23. Wang Z, Liu S, Kakizaki M, Hirose Y, Ishikawa Y, Funato H, Yanagisawa M, Yu Y, Liu Q. Orexin/hypocretin activates mTOR complex 1 (mTORC1) via an Erk/Akt-independent and calcium-stimulated lysosome v-ATPase pathway. J Biol Chem 2014;289:31950–31959.

24. Casare F, Milan D, Fernandez R. Stimulation of calcium-sensing receptor increases biochemical H(+)-ATPase activity in mouse cortex and outer medullary regions. Can J Physiol Pharmacol 2014;92:181–188.

25. Wang Y, Subramanian M, Yurdagul A Jr, Barbosa-Lorenzi VC, Cai B, de Juan-Sanz J, Ryan TA, Nomura M, Maxfield FR, Tabas I. Mitochondrial fission promotes the continued clearance of apoptotic cells by macrophages. Cell 2017;171:331–345 e22.

26. Morita M, Prudent J, Basu K, Goyon V, Katsumura S, Hulea L, Pearl D, Siddiqui N, Strack S, McGuirk S, St-Pierre J, Larsson O, Topisirovic I, Vali H, McBride HM, Bergeron JJ, Sonenberg N. mTOR controls mitochondrial dynamics and cell survival via MTFP1. Mol Cell 2017;67:922–935 e5.

27. Chang CR, Blackstone C. Dynamic regulation of mitochondrial fission through modification of the dynamin-related protein Drp1. Ann N Y Acad Sci 2010; 1201:34–39.

28. Tol MJ, Ottenhoff R, van Eijk M, Zelcer N, Aten J, Houten SM, Geerts D, van Roomen C, Bierlaagh MC, Scheij S, Hoeksema MA, Aerts JM, Bogan JS, Dorn GW 2nd, Argmann CA, Verhoeven AJ. A PPARgamma-Bnip3 axis couples adipose mitochondrial fusion-fission balance to systemic insulin sensitivity. Diabetes 2016;65:2591–2605.

29. Marsboom G, Toth PT, Ryan JJ, Hong Z, Wu X, Fang YH, Thenappan T, Piao L, Zhang HJ, Pogoriler J, Chen Y, Morrow E, Weir EK, Rehman J, Archer SL. Dynamin-related protein 1-mediated mitochondrial mitotic fission permits hyperproliferation of vascular smooth muscle cells and offers a novel therapeutic target in pulmonary hypertension. Circ Res 2012; 110:1484–1497.

30. Roy S, Esmaeilniakooshkghazi A, Patnaik S, Wang Y, George SP, Ahrorov A, Hou JK, Herron AJ, Sesaki H, Khurana S. Villin-1 and gelsolin regulate changes in actin dynamics that affect cell survival signaling pathways and intestinal inflammation. Gastroenterology 2018; 154:1405–1420 e2.

31. Cui M, Tang X, Christian WV, Yoon Y, Tieu K. Perturbations in mitochondrial dynamics induced by human mutant PINK1 can be rescued by the mitochondrial division inhibitor mdivi-1. J Biol Chem 2010; 285:11740–11752.

32. Yamanaka K, Petrulionis M, Lin S, Lin S, Gao C, Galli U, Richter S, Winkler S, Houben P, Schultze D, Hatano E, Schemmer P. Therapeutic potential and adverse events of everolimus for treatment of hepatocellular carcinoma - systematic review and meta-analysis. Cancer Med 2013; 2:862–871.

33. Schuster S, Cabrera D, Arrese M, et al. Triggering and resolution of inflammation in NASH. Nat Rev Gastroenterol Hepatol 2018;15:349–364.

34. Ni Y, Nagashimada M, Zhuge F, Feldstein AE. Astaxanthin prevents and reverses diet-induced insulin resistance and steatohepatitis in mice: a comparison with vitamin E. Sci Rep 2015;5:17192.

35. Han YH, Kim HJ, Na H, Nam MW, Kim JY, Kim JS, Koo SH, Lee MO. RORalpha induces KLF4-mediated M2 polarization in the liver macrophages that protect against nonalcoholic steatohepatitis. Cell Rep 2017;20:124–135.

36. Fan Z, Li L, Li M, Zhang X, Hao C, Yu L, Zeng S, Xu H, Fang M, Shen A, Jenuwein T, Xu Y. The histone methyltransferase Suv39h2 contributes to nonalcoholic steatohepatitis in mice. Hepatology 2017;65:1904–1919.

37. Wan J, Benkdane M, Teixeira-Clerc F, Bonnafous S, Louvet A, Lafdil F, Pecker F, Tran A, Gual P, Mallat A, Lotersztajn S, Pavoine C. M2 Kupffer cells promote M1 Kupffer cell apoptosis: a protective mechanism against alcoholic and nonalcoholic fatty liver disease. Hepatology 2014;59:130–142.

38. Zhu L, Yang T, Li L, Sun L, Hou Y, Hu X, Zhang L, Tian H, Zhao Q, Peng J, Zhang H, Wang R, Yang Z, Zhang L, Zhao Y. TSC1 controls macrophage polarization to prevent inflammatory disease. Nat Commun 2014;5:4696.

39. Byles V, Covarrubias AJ, Ben-Sahra I, Lamming DW, Sabatini DM, Manning BD, Horng T. The TSC-mTOR pathway regulates macrophage polarization. Nat Commun 2013;4:2834.

40. Hong Z, Kutty S, Toth PT, Marsboom G, Hammel JM, Chamberlain C, Ryan JJ, Zhang HJ, Sharp WW, Morrow E, Trivedi K, Weir EK, Archer SL. Role of dynamin-related protein 1 (Drp1)-mediated mitochondrial fission in oxygen sensing and constriction of the ductus arteriosus. Circ Res 2013;112:802–815.

41. Devisscher L, Scott CL, Lefere S, Raevens S, Bogaerts E, Paridaens A, Verhelst X, Geerts A, Guilliams M, Van Vlierberghe H. Non-alcoholic steatohepatitis induces transient changes within the liver macrophage pool. Cell Immunol 2017;322:74–83.

42. Liu K, Zhao E, Ilyas G, Lalazar G, Lin Y, Haseeb M, Tanaka KE, Czaja MJ. Impaired macrophage autophagy increases the immune response in obese mice by promoting proinflammatory macrophage polarization. Autophagy 2015;11:271–284.

43. Bagh MB, Peng S, Chandra G, Zhang Z, Singh SP, Pattabiraman N, Liu A, Mukherjee AB. Misrouting of v-ATPase subunit V0a1 dysregulates lysosomal acidification in a neurodegenerative lysosomal storage disease model. Nat Commun 2017;8:14612.

44. Graf R, Harvey WR, Wieczorek H. Purification and properties of a cytosolic V1-ATPase. J Biol Chem 1996; 271:20908–20913.

45. Luchsinger LL, de Almeida MJ, Corrigan DJ, Mumau M, Snoeck HW. Mitofusin 2 maintains haematopoietic stem cells with extensive lymphoid potential. Nature 2016; 529:528–531.

46. Wang S, Tsun ZY, Wolfson RL, Shen K, Wyant GA, Plovanich ME, Yuan ED, Jones TD, Chantranupong L, Comb W, Wang T, Bar-Peled L, Zoncu R, Straub C, Kim C, Park J, Sabatini BL, Sabatini DM. Metabolism. Lysosomal amino acid transporter SLC38A9 signals arginine sufficiency to mTORC1. Science 2015; 347:188–194.

47. Wong YC, Ysselstein D, Krainc D. Mitochondria-lysosome contacts regulate mitochondrial fission via RAB7 GTP hydrolysis. Nature 2018;554:382–386.

48. Keirsse J, Van Damme H, Geeraerts X, Beschin A, Raes G, Van Ginderachter JA. The role of hepatic

macrophages in liver metastasis. Cell Immunol 2018; 330:202–215.

49. Takegoshi K, Honda M, Okada H, Takabatake R, Matsuzawa-Nagata N, Campbell JS, Nishikawa M, Shimakami T, Shirasaki T, Sakai Y, Yamashita T, Takamura T, Tanaka T, Kaneko S. Branched-chain amino acids prevent hepatic fibrosis and development of hepatocellular carcinoma in a non-alcoholic steatohepatitis mouse model. Oncotarget 2017;8:18191–18205.

50. Kleiner DE, Brunt EM, Van Natta M, Behling C, Contos MJ, Cummings OW, Ferrell LD, Liu YC, Torbenson MS, Unalp-Arida A, Yeh M, McCullough AJ, Sanyal AJ; Nonalcoholic Steatohepatitis Clinical Research Network. Design and validation of a histological scoring system for nonalcoholic fatty liver disease. Hepatology 2005;41:1313–1321.

51. Wang X, Zheng Z, Caviglia JM, Corey KE, Herfel TM, Cai B, Masia R, Chung RT, Lefkowitch JH, Schwabe RF, Tabas I. Hepatocyte TAZ/WWTR1 promotes inflammation and fibrosis in nonalcoholic steatohepatitis. Cell Metab 2016;24:848–862.

52. Yao L, Wang C, Zhang X, Peng L, Liu W, Zhang X, Liu Y, He J, Jiang C, Ai D, Zhu Y. Hyperhomocysteinemia activates the aryl hydrocarbon receptor-CD36 pathway to promote hepatic steatosis in mice. Hepatology 2016; 64:92–105.

53. Canbay A, Feldstein AE, Higuchi H, Werneburg N, Grambihler A, Bronk SF, Gores GJ. Kupffer cell engulfment of apoptotic bodies stimulates death ligand and cytokine expression. Hepatology 2003; 38:1188–1198.

54. Fazal L, Laudette M, Paula-Gomes S, Pons S, Conte C, Tortosa F, Sicard P, Sainte-Marie Y, Bisserier M, Lairez O, Lucas A, Roy J, Ghaleh B, Fauconnier J, Mialet-Perez J, Lezoualc'h F. Multifunctional mitochondrial Epac1 controls myocardial cell death. Circ Res 2017; 120:645–657.

Correspondence
Address correspondence to: Ding Ai, PhD, or Chunjiong Wang, MD, Department of Physiology and Pathophysiology, Tianjin Medical University, Tianjin, 300070, China. e-mail: edin2000cn@163.com or wangchunjiong@126.com; fax: 86-22-83336565.

Author contributions
Wenli Liu and Chenji Ye contributed to the concept and design, data acquisition, analysis and interpretation of data and drafting of the article; Qian Cheng, Xuejiao Zhang, Liu Yao, Qi Li, Jing Huang, Yajin Liu, Zhengsheng Zou, Hua Wang, and Jun Yan acquired date for the article; Yi Zhu contributed to the concept and design of the article; Chunjiong Wang and Ding Ai contributed to the concept and design, data acquisition, analysis and interpretation of data, and drafting of the article; Ding Ai and Chunjiong Wang are the guarantors of the work; and all authors approved the final version of the article.

Conflicts of interest
The authors disclose no conflicts.